analysis using anti-V5 and anti-GFP antibodies. Bands for expressed proteins are indicated by arrowheads. Note that gel top bands (indicated by arrows) were observed for Tcf20 (1~400 or 1~500)-V5 and NF-YA-V5 but not for LacZ-V5 by co-expression of Nhtt150Q-EGFP, suggesting their co-insolubilization with mutant Nhtt in neuro2a cells. (E) Nhtt150Q-EGFP cells were transfected with expression vectors for Tcf20 (full, 1~400 or 1~500)-V5 together with pRFP-C1 vector. After one day, cells were treated with ponasterone A for 24 hr and the cells with aggregates in trasnfected (RFP-positive) cells were quantified by ArrayScan reader. Ratios to control (empty vector) are shown. Values are means ± SD of four well data (**P<0.01). Scale bars are 10 μm (B, C).
doi:10.1371/journal.pone.0093891.g006

found in this study are found as modifiers of toxicity in polyglutamine disease models, such as Trappc9 [34], Casp3 [64], Gnfl (*Drosophila* Rfc1) [65], and F40F8.1 (*C. elegans* Cmpk1) [66]. Notably, gene expression array analysis using R6/2 HD model mice (T.Y and N.N. unpublished data) suggests that some of the shRNA target genes show altered expression in R6/2 brain cortex. These include Rab2b (129% to the control, $P=0.0016$), Klhl7 (121%, $P=0.0050$), Fkbp9 (122%, $P=0.0098$), Plp2 (72.6%, $P=0.0023$), Mei1 (82.1%, $P=0.0208$), Pip5k1b (73.6%, $P=4.74E-04$) and Rassf4 (80.7%, $P=4.58E-04$). These observations suggest potential *in vivo* significance of these genes for regulation of mutant polyQ aggregation. Further studies are needed to understand the molecular mechanisms underlying regulation of mutant Htt aggregation/toxicity by the modifiers identified in this study.

In summary, through shRNA screening using neuro2a cells, here we identified novel mammalian modifiers of mutant Htt aggregation. Our data suggest that several modifiers mediate their effect possibly through proteasome-independent mechanism such as direct interaction with mutant Htt and protein phosphorylation pathways involving casein kinases and PI kinases. Further studies focused on our identified modifiers may deepen our understanding on the molecular mechanism of mutant Htt aggregation and lead to identification of potential therapeutic targets of HD and other polyglutamine diseases.

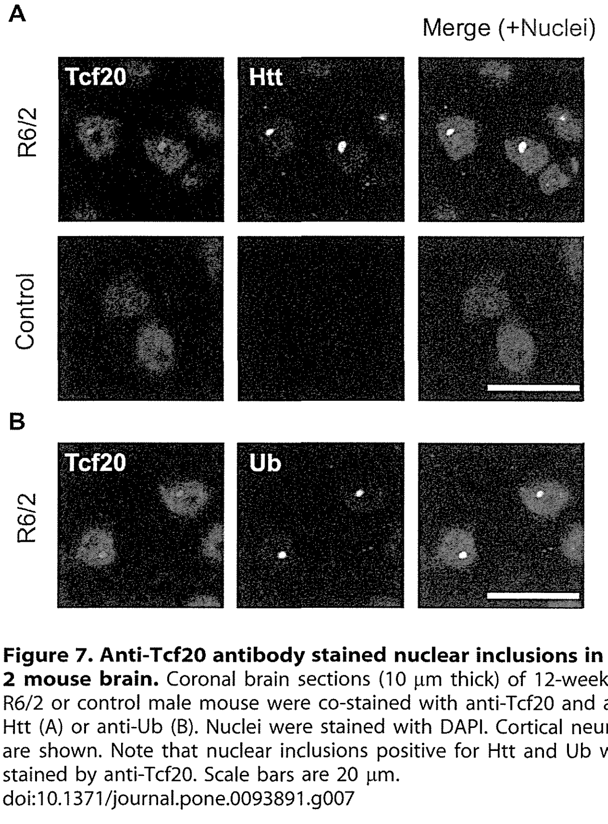

Figure 7. Anti-Tcf20 antibody stained nuclear inclusions in R6/2 mouse brain. Coronal brain sections (10 μm thick) of 12-week-old R6/2 or control male mouse were co-stained with anti-Tcf20 and anti-Htt (A) or anti-Ub (B). Nuclei were stained with DAPI. Cortical neurons are shown. Note that nuclear inclusions positive for Htt and Ub were stained by anti-Tcf20. Scale bars are 20 μm.
doi:10.1371/journal.pone.0093891.g007

Materials and Methods

Cell lines

Neuro2a mouse neuroblastome cells, a gift from Dr Iwatsubo (Tokyo University) [35], were maintained in DMEM supplemented with 10% FBS and penicillin-streptomycin in an atmosphere containing 5% CO_2. Stably transfected neuro2a cells, which inducibly express N-terminal Htt (exon 1) containing 16Q or 150Q fusing EGFP (Nhtt16Q-EGFP or Nhtt150Q-EGFP) under control of ponasterone A, were cultured as above but the medium was further supplemented with 0.4 mg/ml of Zeocin and 0.2 mg/ml of G418 as described previously [35,46]. Note that Zeocin and G418 were only used for cell maintenance but not for cell transfection experiments described blow.

Mouse shRNA library

Mouse shRNA libraries (Mouse shRNAmir retroviral library; release 2.3~2.7 and 2.15) were purchased from Open Biosystems. In this system, shRNAs, cloned in pSHAG-MAGIC2 (pSM2) vector, are expressed under U6 promoter as human microRNA-30 (miR30) primary transcripts and efficiently processed by Drosha and Dicer to produce shRNA. Because the vector contains puromycin resistant gene, the shRNA-expressing cells were able to be selected by treatment the cells with puromycin. The shRNA clones were provided as frozen glycerol stock of E. coli (DH10beta pir116Frt) in 96 well plates. We first amplified the clones in LB medium in 96 well culture plates and purified plasmid DNA by using a plasmid DNA collection system Biomek FX (Beckman Coulter) accompanied with Wizard MagneSil Tfx system (Promega). Clones with no or few growth were excluded at this point. Purities of the clones were estimated by checking their OD260/280 ratio. At least 4~5 clones in each plate were randomly picked up and subjected to agarose gel electrophoresis to check the DNA integrity.

shRNA screening using Nhtt-EGFP cell lines

Stable cells for Nhtt16Q-EGFP or Nhtt150Q-EGFP were seeded on 96 well plates in 50 μl of culture medium (10% FBS/DMEM) at density of 2.5×10^4 cells per well. On the next day, the cells were transfected by adding 15 μl Opti-MEM containing 100 ng of shRNA plasmid DNA and 0.2 μl Lipofectamine 2000 (Invitrogen) to the wells. After 5 hr, 50 μl of medium containing dibutyryl cyclic AMP (dcAMP; final conc. 5 mM) was added to the well. After overnight incubation, the medium was replaced to one containing 2.5 μg/ml puromycin and 5 mM dcAMP for selection of shRNA-expressing cells. After 24 hr incubation, the medium was replaced to one containing 1 μM of ponasterone A and 5 mM dcAMP to induce Nhtt-EGFP expression. After 24 hr, cells were fixed and subjected to nuclear staining with Hoechst or DAPI. The fluorescence cell images in same area of each well were automatically obtained and analyzed by ArrayScan HCS Reader (Cellomics, Thermo Fisher Scientific) along with the protocols designed by the instruction manual. For data analysis of Nhtt150Q-EGFP cells, cells with strong EGFP intensities were counted as aggregate-containing cells because the aggregation accompanied accumulated EGFP signal in the cells. We then

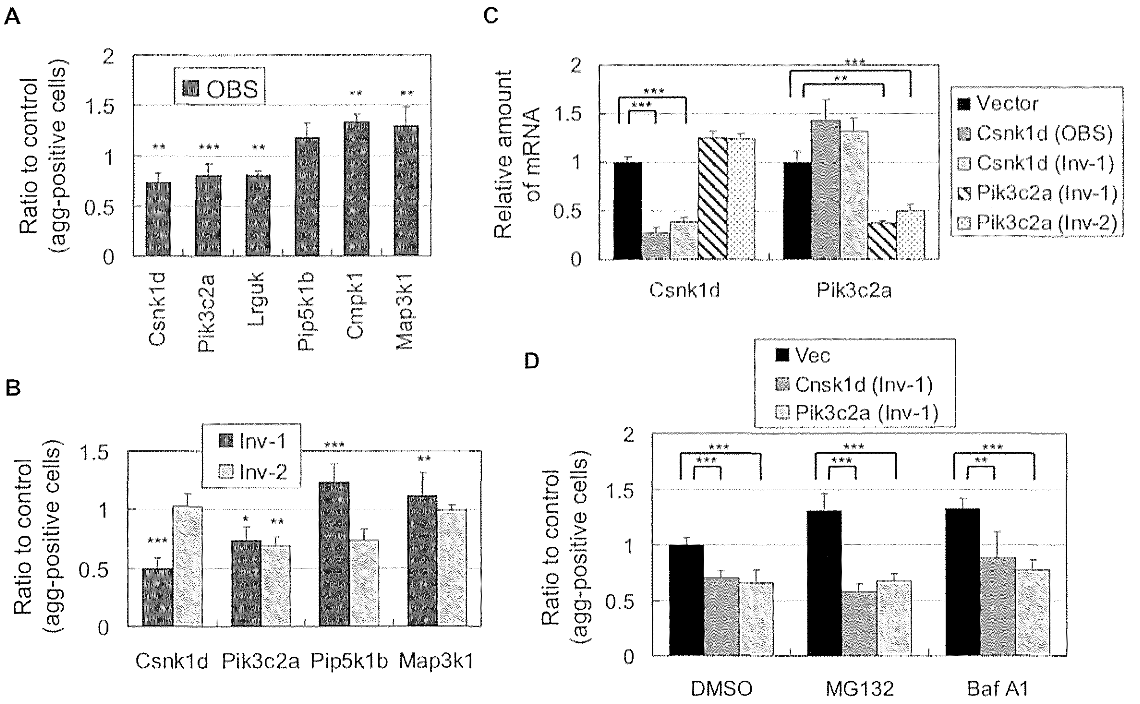

Figure 8. Kinases whose knockdown modifies Nhtt150Q-EGFP aggregation in neuro2a cells. (A, B) Nhtt150Q-EGFP cells were transfected with miRNA expression vector. After 2 days, cells were treated with ponasterone A for 24 hr and the cells with aggregates in miRNA trasnfected cells were quantified by ArrayScan reader. Ratios to control (empty vector) are shown. Note the reproduction of the shRNA's effect by miRNA binding to same sequence (OBS) (A) or difference sequences (Inv-1 or -2) (B). (C) Neuro2a cells expressing indicated miRNAs were subjected to quantitative RT-PCR. (D) Nhtt150Q-EGFP cells expressing indicated miRNAs were treated with 0.5 μM MG132, 0.2 μM Baf A1 or DMSO for 24 hr, and the cells with aggregates were quantified as above. Ratios to control (empty vector) are shown. Values are means ± SD of at least three well data (A–C) or six well data (D) (*$P<0.05$, **$P<0.01$, ***$P<0.001$).
doi:10.1371/journal.pone.0093891.g008

divided the number of aggregate-containing cells by total number of cells estimated by counting stained nuclei in the same field, and calculated percentage of cells with aggregates. For data analysis of Nhtt16Q-EGFP cells, EGFP intensities in each cell were quantified and averaged by ArrayScan reader. In both analyses, at least 1000 cells (2000~3000 cells in average) were analyzed for each well. Scheme of screening procedure is described in Figure 1.

miRNA construction and gene knockdown

Invitrogen miRNAs (miR RNAi) were designed by BLOCK-iT RNAi Designer in Invitrogen's Web site. Oligo DNAs used for miRNA constructions were listed in Table S1. These were cloned into pcDNA6.2-mRFP-miR vector [36]. By using this vector, transfected cells expressing miRNA were detected by mRFP fluorescence. For gene knockdown, Nhtt150Q-EGFP cells seeded on 24 well plates were transfected with 0.4 μg of miRNA vector by Lipofectamine 2000 (Invitrogen), according to the manufacturer's protocol. After 5 hr of transfection, medium was replaced to one containing 5 mM dcAMP and cells were further incubated for 2 days. Then, the cells were incubated with 1 μM of ponasterone A for 24 hr to induce Nhtt150Q-EGFP expression. The cells were fixed and analyzed by ArrayScan reader and in this case, cells with Nhtt150Q-EGFP aggregates in RFP-positive, miRNA-transfected cells were quantified.

Treatment of cells with MG132 or Baf A1

Transfection of Nhtt150Q-EGFP cells with shRNA or miRNA was performed as described above. MG132 (Chalbochem) or Baf A1 (LC Laboratories) was co-added to the medium with ponasterone A. After 24 hr incubation, the cells were fixed and cells with aggregates were quantified as above.

cDNA expression vectors and cell transfection

The mouse cDNAs for full-length Rab2b (clone ID: 4930528G15) and partial regions of Ddr2 (4732470C17) and Tcf20 (4930548B22, I830053D05) were kindly provided as FANTOM3 clones [67]. Remaining regions of Ddr2 and Tcf20 were obtained by RT-PCR to make full-CDS cDNAs. By using Gateway system, these cDNAs were subcloned into the pcDNA-DEST40 vector that expresses cDNA product as C-terminal V5-His tagged protein (Invitrogen). Expression vectors for Tcf20 containing 1~400 or 1~500 amino acid were constructed by insertion of their fragments amplified by PCR into pcDNA3.1-V5His vector. Vectors for Nhtt16Q-EGFP, Nhtt150Q-EGFP or Nhtt150Q-EGFP-NLS in pcDNA3.1 vector (Invitrogen) were described previously [35,46], and pcDNA3.1-LacZ-V5His vector was obtained from Invitrogen. To examine the interaction of the modifiers with mutant Nhtt [12], neuro2a cells were transfected with above expression vectors by Lipofectamine 2000 (Invitrogen) and incubated for one day, For immunofluorescence staining, the cells were fixed with 4% PFA/PBS, permeabilized with 0.1% triton X-100/TBST (20 mM Tris-HCl, pH 8.0, 150 mM NaCl, 0.05% Tween20), and blocked with 5% goat serum/TBST. The cells were then incubated with anti-V5 (R960-25, Invitrogen) diluted with TBST containing 0.1% bovine serum albumin (BSA) for overnight at 4°C, followed by incubation with Alexa 546-conjugated anti-mouse IgG (Molecular Probes). The cells were then mounted in VECTASHIELD with DAPI (VECTOR) and

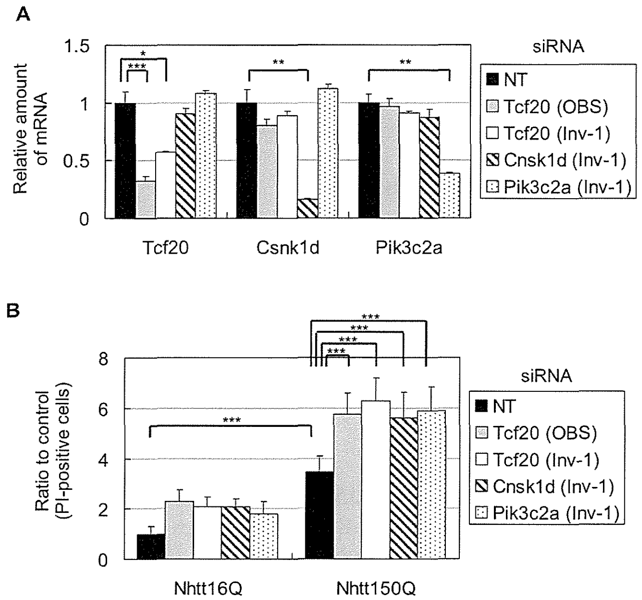

Figure 9. Effect of knockdown of aggregation-modifiers on mutant Nhtt-induced cell toxicity. (A) Neuro2a cells were transfected with siRNAs for NT (non-targeting), Tcf20 (OBS or Inv-1), Csnk1d (Inv-1) or Pik3c2a (Inv-1). After two days, the cells subjected to quantitative RT-PCR. Specific and significant reduction of their target mRNAs was observed. Values are means ± SD of three well data (**P*< 0.05, ***P*<0.01, *** *P*<0.001). (B) siRNA-transduced neuro2a cells were further transfected with expression vector for Nhtt16Q-EGFP or Nhtt150Q-EGFP. After two days, the cells were co-stained with PI and Hoechst and subjected to ArrayScan analysis to count PI-positive dead cells among the cells positive for both Hoechst and GFP. Ratios to control (NT siRNA- and Nhtt16Q-EGFP-transfected cells) were shown. Values are means ± SD of eight well data (****P*<0.001).
doi:10.1371/journal.pone.0093891.g009

analyzed by Leica confocal system (TCS SP2, SP5). For Western blot analysis, the cells were boiled in SDS sample buffer and subjected to Western blotting as described previously [68]. Primary antibodies used were anti-V5 and anti-GFP (04363, nacalai). Chemiluminescent signals were obtained and quantified using ImageQuant LAS-4000 (GE). To examine the effect of Tcf20 overexpression on mutant Nhtt aggregation, Nhtt150Q-EGFP cells were transfected with expression vectors for Tcf20 (full, 1~400 or 1~500)-V5 together with pRFP-C1 vector. The cells were then differentiated by dcAMP on the same day and treated with ponasterone A on the next day. After 24 hr, the cells were fixed and cells with aggregates in trasnfected (RFP-positive) cells were quantified by ArrayScan reader.

Immunofluorescence staining of mouse brain sections

The mouse experiments were approved by the animal experiment committee at RIKEN Brain Science Institute. Mice were maintained and bred in accordance with RIKEN guidelines. Heterozygous htt exon 1 transgenic male mice of the R6/2 strain were obtained from Jackson Laboratory (Bar Harbor, ME) and maintained as B6CBAF1 background. In this paper, R6/2 male mice and age-matched littermates were used for experiments. For immunofluorescence staining [12], frozen raw brains were cut into 10 μm sections. After fixing with 4% PFA/PBS, the sections were treated with 0.01% H_2O_2/methanol at room temperature for 30 min and blocked with 5% skim milk/TBST for 1 hr. The sections were then incubated with a primary antibody diluted with 0.1% BSA/TBST for overnight at 4°C, followed by incubation with a secondary antibody conjugated with Alexa Fluor dyes (Molecular Probes). Primary antibodies used were anti-Htt (EM48; MAB5374, Chemicon), anti-Ub (FK2, BML-PW8810, Enzo) and anti-Tcf20 (sc-86878, Santa Cruz). The tissues were mounted in VECTASHIELD with DAPI and analyzed by a Leica confocal system (TCS SP5).

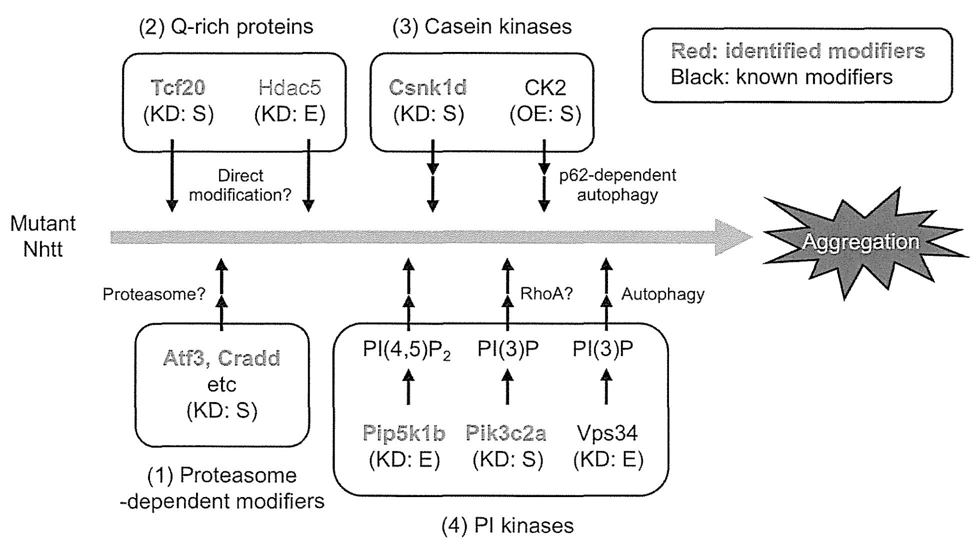

Figure 10. Scheme of modification of mutant Nhtt aggregation by genes identified by shRNA screening. Our experimental data suggest that the genes identified here (indicated by red) modify the mutant Nhtt aggregation by several mechanisms. (1) Proteasome-dependent modification involving Atf3 and Cardd whose knockdown (KD) both suppress the aggregation. (2) Potential direct modification by Q-rich proteins such as Tcf20 and Hdac5, whose knockdown suppresses or enhances the aggregation, respectively. (3) Casein kinase-mediated modification involving Csnk1d whose knockdown suppresses the aggregation. In contrast, overexpression (OE) of CK2 is reported to reduce the aggregates by accelerating p62-dependent autophagic clearance. (4) PI kinase-mediated modification involving Pik3c2a and Pip5k1b, whose knockdown suppresses or enhances the aggregation, respectively. In contrast, knockdown of Vps34, a class III PI3K, is reported to increase the aggregates by attenuating autophagic clearance. The S and E indicate suppression and enhancement of the mutant Nhtt aggregation, respectively.
doi:10.1371/journal.pone.0093891.g010

Quantitative reverse transcription (RT)-PCR

Preparations of total RNA, reverse transcription and cDNA synthesis from neuro2a cells were performed as described previously [6]. We used following primers designed by Primer Express software (Applied Biosystems) for quantitative PCR; Csnk1d (GCACGCTATGCCTCCATCA, ACCCCAGA-GACTCCAAGTCATC), Gapdh (TGTGTCCGTCGTGGATCTGA, CCTGCTTCAC-CACCTTCTTGA) and Pik3c2a (TTCATAACCTTGCT-CAGCTACGTT, GATCCGGCCATCTTGTCTAAAG). Quantitative PCR was performed by SYBR green according to the manufacturer's protocol (Applied Biosystems or Roche). All values obtained were normalized with respect to levels of Gapdh mRNA.

siRNA transfection and cell toxicity assay

siRNAs were designed based on miRNA target sequences (Table S1) and synthesized by Nippon Gene as 3′ dTdT overhangs. The siRNA sequences without overhangs are follows; no-targeting control (NT) (uagcgacuaaacacaucaa), Tcf20-OBS (gauaucaagucauuuccua), Tcf20-Inv-1 (ccuauaaguguggcgcuuc), Csnk1d-Inv-1 (gcuccuucggagacaucua) and Pik3c2a-Inv-1 (uccugc-guuugacauuauu). These were transduced into cells using RNAi-MAX (Invitrogen) according to the manufacture's protocol. After one day, the cells were transfected with expression vector for Nhtt16Q-EGFP or Nhtt150Q-EGFP using Lipofectamin 2000 and further incubated for two days in the medium containing 5 mM dcAMP. Then, the cells were co-incubated with 10 μM pyridinium iodide (PI) and 10 μg/ml Hoechst 33342 for 10 min and analyzed by ArrayScan reader. Percent of dead cells in Nhtt-expressing cells was calculated by counting PI-positive cells in the cells positive for both Hoechst and GFP.

Gene classification

Target genes of final 111 shRNAs were classified using PANTHER Classification System (http://www.pantherdb.org) [37]. Ensembl gene IDs (Data S1) were used as inputs for the analysis. The genes were classified based on their molecular function, biological process, and PANTHER protein class. We also performed Statistical Overrepresentation Test for these genes to examine enrichment of GO term or pathway.

Statistical analysis

For comparison between two sample groups, data were first analyzed by F-test. For $P>0.05$, the data were analyzed by unpaired Student's t-test (two-tailed); otherwise data were analyzed by Welch's t-test (two-tailed). We considered the difference between comparisons to be significant when $P<0.05$ for all statistical analyses except of third screening in which shRNAs with $P<0.1$ were also included as candidates.

Supporting Information

Data S1 Complete list of the screening data for final 111 shRNAs. Clone IDs, targets genes and data sets of first, second and third screening for final 111 shRNAs are listed. Clone IDs are originally named in this paper based on the plate number and well position of the shRNA. MGI Gene IDs, Ensembl IDs and Entrez Gene IDs in MGI database, and Oligo IDs, Accessions and shRNA sequences in supplemented Open Biosystems (OBS) database are also described.
(XLS)

Data S2 Sequences of cDNAs used for miRNA construction. cDNA sequences of shRNA target genes used for miRNA construction. Binding sequences of shRNAs (OBS) are labeled with blue, whereas those of miRNAs (Inv-1/2) are labeled with yellow. Coding DNA Sequences (CDS) are underlined. Note that miRNA-binding sequences are completely different from those of shRNAs except of Gnpda1 in which partial overlap (labeled with green) is observed.
(PDF)

Table S1 *List of the oligos used for miRNA construction.* OBS means the oligos designed based on Open Biosystems shRNA sequence. Inv-1/2 means the oligos designed by BLOCK-iTTM RNAi Designer in Invitrogen's Web site. Number in parenthesis indicates starting position of miRNA-target sequence in coding sequence.
(PDF)

Acknowledgments

We thank the staff at the RRC (RIKEN BSI) for technical support, the FANTOM consortium for FANTOM clones and lab members of RIKEN BSI for technical help.

Author Contributions

Conceived and designed the experiments: TY HKW NN. Performed the experiments: AT TY HKW POB KW MK. Analyzed the data: TY HKW AT. Contributed reagents/materials/analysis tools: NH TS. Wrote the paper: TY HKW NN.

References

1. Bauer PO, Nukina N (2009) The pathogenic mechanisms of polyglutamine diseases and current therapeutic strategies. J Neurochem 110: 1737–1765.
2. Imarisio S, Carmichael J, Korolchuk V, Chen CW, Saiki S, et al. (2008) Huntington's disease: from pathology and genetics to potential therapies. Biochem J 412: 191–209.
3. Li SH, Li XJ (2004) Huntingtin-protein interactions and the pathogenesis of Huntington's disease. Trends Genet 20: 146–154.
4. Harjes P, Wanker EE (2003) The hunt for huntingtin function: interaction partners tell many different stories. Trends Biochem Sci 28: 425–433.
5. Yamanaka T, Miyazaki H, Oyama F, Kurosawa M, Washizu C, et al. (2008) Mutant Huntingtin reduces HSP70 expression through the sequestration of NF-Y transcription factor. Embo J 27: 827–839.
6. Yamanaka T, Tosaki A, Miyazaki H, Kurosawa M, Furukawa Y, et al. (2010) Mutant huntingtin fragment selectively suppresses Brn-2 POU domain transcription factor to mediate hypothalamic cell dysfunction. Hum Mol Genet 19: 2099–2112.
7. Yamanaka T, Tosaki A, Kurosawa M, Matsumoto G, Koike M, et al. (2014) NF-Y inactivation causes atypical neurodegeneration characterized by ubiquitin and p62 accumulation and endoplasmic reticulum disorganization. Nat Commun 5: 3354.
8. Doi H, Okamura K, Bauer PO, Furukawa Y, Shimizu H, et al. (2008) RNA-binding protein TLS is a major nuclear aggregate-interacting protein in huntingtin exon 1 with expanded polyglutamine-expressing cells. J Biol Chem 283: 6489–6500.
9. Furukawa Y, Kaneko K, Matsumoto G, Kurosawa M, Nukina N (2009) Cross-seeding fibrillation of Q/N-rich proteins offers new pathomechanism of polyglutamine diseases. J Neurosci 29: 5153–5162.
10. Cha JH (2000) Transcriptional dysregulation in Huntington's disease. Trends Neurosci 23: 387–392.
11. Sugars KL, Rubinsztein DC (2003) Transcriptional abnormalities in Huntington disease. Trends Genet 19: 233–238.
12. Yamanaka T, Nukina N (2010) Transcription factor sequestration by polyglutamine proteins. Methods Mol Biol 648: 215–229.
13. Wacker JL, Zareie MH, Fong H, Sarikaya M, Muchowski PJ (2004) Hsp70 and Hsp40 attenuate formation of spherical and annular polyglutamine oligomers by partitioning monomer. Nat Struct Mol Biol 11: 1215–1222.
14. Muchowski PJ, Schaffar G, Sittler A, Wanker EE, Hayer-Hartl MK, et al. (2000) Hsp70 and hsp40 chaperones can inhibit self-assembly of polyglutamine proteins into amyloid-like fibrils. Proc Natl Acad Sci U S A 97: 7841–7846.

15. Fujimoto M, Takaki E, Hayashi T, Kitaura Y, Tanaka Y, et al. (2005) Active HSF1 significantly suppresses polyglutamine aggregate formation in cellular and mouse models. J Biol Chem 280: 34908–34916.
16. Kazemi-Esfarjani P, Benzer S (2000) Genetic suppression of polyglutamine toxicity in Drosophila. Science 287: 1837–1840.
17. Chan HY, Warrick JM, Gray-Board GL, Paulson HL, Bonini NM (2000) Mechanisms of chaperone suppression of polyglutamine disease: selectivity, synergy and modulation of protein solubility in Drosophila. Hum Mol Genet 9: 2811–2820.
18. Wacker JL, Huang SY, Steele AD, Aron R, Lotz GP, et al. (2009) Loss of Hsp70 exacerbates pathogenesis but not levels of fibrillar aggregates in a mouse model of Huntington's disease. J Neurosci 29: 9104–9114.
19. Behrends C, Langer CA, Boteva R, Bottcher UM, Stemp MJ, et al. (2006) Chaperonin TRiC promotes the assembly of polyQ expansion proteins into nontoxic oligomers. Mol Cell 23: 887–897.
20. Kitamura A, Kubota H, Pack CG, Matsumoto G, Hirayama S, et al. (2006) Cytosolic chaperonin prevents polyglutamine toxicity with altering the aggregation state. Nat Cell Biol 8: 1163–1170.
21. Tam S, Geller R, Spiess C, Frydman J (2006) The chaperonin TRiC controls polyglutamine aggregation and toxicity through subunit-specific interactions. Nat Cell Biol 8: 1155–1162.
22. Nagai Y, Fujikake N, Ohno K, Higashiyama H, Popiel HA, et al. (2003) Prevention of polyglutamine oligomerization and neurodegeneration by the peptide inhibitor QBP1 in Drosophila. Hum Mol Genet 12: 1253–1259.
23. Nagai Y, Tucker T, Ren H, Kenan DJ, Henderson BS, et al. (2000) Inhibition of polyglutamine protein aggregation and cell death by novel peptides identified by phage display screening. J Biol Chem 275: 10437–10442.
24. Sanchez I, Mahlke C, Yuan J (2003) Pivotal role of oligomerization in expanded polyglutamine neurodegenerative disorders. Nature 421: 373–379.
25. Tanaka M, Machida Y, Niu S, Ikeda T, Jana NR, et al. (2004) Trehalose alleviates polyglutamine-mediated pathology in a mouse model of Huntington disease. Nat Med 10: 148–154.
26. Liu CR, Chang CR, Chern Y, Wang TH, Hsieh WC, et al. (2012) Spt4 is selectively required for transcription of extended trinucleotide repeats. Cell 148: 690–701.
27. Silva MC, Fox S, Beam M, Thakkar H, Amaral MD, et al. (2011) A genetic screening strategy identifies novel regulators of the proteostasis network. PLoS Genet 7: e1002438.
28. Garcia SM, Casanueva MO, Silva MC, Amaral MD, Morimoto RI (2007) Neuronal signaling modulates protein homeostasis in Caenorhabditis elegans post-synaptic muscle cells. Genes Dev 21: 3006–3016.
29. van Ham TJ, Holmberg MA, van der Goot AT, Teuling E, Garcia-Arencibia M, et al. (2010) Identification of MOAG-4/SERF as a regulator of age-related proteotoxicity. Cell 142: 601-612.
30. Nollen EA, Garcia SM, van Haaften G, Kim S, Chavez A, et al. (2004) Genome-wide RNA interference screen identifies previously undescribed regulators of polyglutamine aggregation. Proc Natl Acad Sci U S A 101: 6403–6408.
31. Doumanis J, Wada K, Kino Y, Moore AW, Nukina N (2009) RNAi screening in Drosophila cells identifies new modifiers of mutant huntingtin aggregation. PLoS One 4: e7275.
32. Weiss KR, Kimura Y, Lee WC, Littleton JT (2012) Huntingtin aggregation kinetics and their pathological role in a Drosophila Huntington's disease model. Genetics 190: 581–600.
33. Zhang S, Binari R, Zhou R, Perrimon N (2010) A genomewide RNA interference screen for modifiers of aggregates formation by mutant Huntingtin in Drosophila. Genetics 184: 1165–1179.
34. Lu B, Al-Ramahi I, Valencia A, Wang Q, Berenshteyn F, et al. (2013) Identification of NUB1 as a suppressor of mutant Huntingtin toxicity via enhanced protein clearance. Nat Neurosci 16: 562–570.
35. Wang GH, Mitsui K, Kotliarova S, Yamashita A, Nagao Y, et al. (1999) Caspase activation during apoptotic cell death induced by expanded polyglutamine in N2a cells. Neuroreport 10: 2435–2438.
36. Matsumoto G, Wada K, Okuno M, Kurosawa M, Nukina N (2011) Serine 403 phosphorylation of p62/SQSTM1 regulates selective autophagic clearance of ubiquitinated proteins. Mol Cell 44: 279–289.
37. Thomas PD, Campbell MJ, Kejariwal A, Mi H, Karlak B, et al. (2003) PANTHER: a library of protein families and subfamilies indexed by function. Genome Res 13: 2129–2141.
38. Jana NR, Dikshit P, Goswami A, Kotliarova S, Murata S, et al. (2005) Co-chaperone CHIP associates with expanded polyglutamine protein and promotes their degradation by proteasomes. J Biol Chem 280: 11635–11640.
39. Iwata A, Nagashima Y, Matsumoto L, Suzuki T, Yamanaka T, et al. (2009) Intranuclear degradation of polyglutamine aggregates by the ubiquitin-proteasome system. J Biol Chem 284: 9796–9803.
40. Thompson LM, Aiken CT, Kaltenbach LS, Agrawal N, Illes K, et al. (2009) IKK phosphorylates Huntingtin and targets it for degradation by the proteasome and lysosome. J Cell Biol 187: 1083–1099.
41. Wong HK, Bauer PO, Kurosawa M, Goswami A, Washizu C, et al. (2008) Blocking acid-sensing ion channel 1 alleviates Huntington's disease pathology via an ubiquitin-proteasome system-dependent mechanism. Hum Mol Genet 17: 3223–3235.
42. Bjorkoy G, Lamark T, Brech A, Outzen H, Perander M, et al. (2005) p62/SQSTM1 forms protein aggregates degraded by autophagy and has a protective effect on huntingtin-induced cell death. J Cell Biol 171: 603–614.
43. Ravikumar B, Vacher C, Berger Z, Davies JE, Luo S, et al. (2004) Inhibition of mTOR induces autophagy and reduces toxicity of polyglutamine expansions in fly and mouse models of Huntington disease. Nat Genet 36: 585–595.
44. Filimonenko M, Isakson P, Finley KD, Anderson M, Jeong H, et al. (2010) The selective macroautophagic degradation of aggregated proteins requires the PI3P-binding protein Alfy. Mol Cell 38: 265–279.
45. Yamamoto A, Cremona ML, Rothman JE (2006) Autophagy-mediated clearance of huntingtin aggregates triggered by the insulin-signaling pathway. J Cell Biol 172: 719–731.
46. Doi H, Mitsui K, Kurosawa M, Machida Y, Kuroiwa Y, et al. (2004) Identification of ubiquitin-interacting proteins in purified polyglutamine aggregates. FEBS Lett 571: 171–176.
47. Goehler H, Lalowski M, Stelzl U, Waelter S, Stroedicke M, et al. (2004) A protein interaction network links GIT1, an enhancer of huntingtin aggregation, to Huntington's disease. Mol Cell 15: 853–865.
48. Jabado O, Wang Q, Rideout HJ, Yeasmin M, Guo KX, et al. (2004) RAIDD aggregation facilitates apoptotic death of PC12 cells and sympathetic neurons. Cell Death Differ 11: 618–630.
49. Murakami T, Shoji M, Imai Y, Inoue H, Kawarabayashi T, et al. (2004) Pael-R is accumulated in Lewy bodies of Parkinson's disease. Ann Neurol 55: 439–442.
50. Corti O, Hampe C, Koutnikova H, Darios F, Jacquier S, et al. (2003) The p38 subunit of the aminoacyl-tRNA synthetase complex is a Parkin substrate: linking protein biosynthesis and neurodegeneration. Hum Mol Genet 12: 1427–1437.
51. Knippschild U, Gocht A, Wolff S, Huber N, Lohler J, et al. (2005) The casein kinase 1 family: participation in multiple cellular processes in eukaryotes. Cell Signal 17: 675–689.
52. Vanhaesebroeck B, Guillermet-Guibert J, Graupera M, Bilanges B (2010) The emerging mechanisms of isoform-specific PI3K signalling. Nat Rev Mol Cell Biol 11: 329–341.
53. Falasca M, Hughes WE, Dominguez V, Sala G, Fostira F, et al. (2007) The role of phosphoinositide 3-kinase C2alpha in insulin signaling. J Biol Chem 282: 28226–28236.
54. Domin J, Gaidarov I, Smith ME, Keen JH, Waterfield MD (2000) The class II phosphoinositide 3-kinase PI3K-C2alpha is concentrated in the trans-Golgi network and present in clathrin-coated vesicles. J Biol Chem 275: 11943–11950.
55. Harris DP, Vogel P, Wims M, Moberg K, Humphries J, et al. (2011) Requirement for class II phosphoinositide 3-kinase C2alpha in maintenance of glomerular structure and function. Mol Cell Biol 31: 63–80.
56. Meunier FA, Osborne SL, Hammond GR, Cooke FT, Parker PJ, et al. (2005) Phosphatidylinositol 3-kinase C2alpha is essential for ATP-dependent priming of neurosecretory granule exocytosis. Mol Biol Cell 16: 4841–4851.
57. Yoshioka K, Yoshida K, Cui H, Wakayama T, Takuwa N, et al. (2012) Endothelial PI3K-C2alpha, a class II PI3K, has an essential role in angiogenesis and vascular barrier function. Nat Med 18: 1560–1569.
58. Bauer PO, Wong HK, Oyama F, Goswami A, Okuno M, et al. (2009) Inhibition of Rho kinases enhances the degradation of mutant huntingtin. J Biol Chem 284: 13153–13164.
59. Liang Y, Jiang H, Ratovitski T, Jie C, Nakamura M, et al. (2009) ATF3 plays a protective role against toxicity by N-terminal fragment of mutant huntingtin in stable PC12 cell line. Brain Res 1286: 221–229.
60. Nonhoff U, Ralser M, Welzel F, Piccini I, Balzereit D, et al. (2007) Ataxin-2 interacts with the DEAD/H-box RNA helicase DDX6 and interferes with P-bodies and stress granules. Mol Biol Cell 18: 1385–1396.
61. Damrath E, Heck MV, Gispert S, Azizov M, Nowock J, et al. (2012) ATXN2-CAG42 sequesters PABPC1 into insolubility and induces FBXW8 in cerebellum of old ataxic knock-in mice. PLoS Genet 8: e1002920.
62. Diaz-Hernandez M, Diez-Zaera M, Sanchez-Nogueiro J, Gomez-Villafuertes R, Canals JM, et al. (2009) Altered P2X7-receptor level and function in mouse models of Huntington's disease and therapeutic efficacy of antagonist administration. FASEB J 23: 1893–1906.
63. Meriin AB, Mabuchi K, Gabai VL, Yaglom JA, Kazantsev A, et al. (2001) Intracellular aggregation of polypeptides with expanded polyglutamine domain is stimulated by stress-activated kinase MEKK1. J Cell Biol 153: 851–864.
64. Miller JP, Yates BE, Al-Ramahi I, Berman AE, Sanhueza M, et al. (2012) A genome-scale RNA-interference screen identifies RRAS signaling as a pathologic feature of Huntington's disease. PLoS Genet 8: e1003042.
65. Vo SH, Butzlaff M, Pru SK, Ni Charthaigh RA, Karsten P, et al. (2012) Large-scale screen for modifiers of ataxin-3-derived polyglutamine-induced toxicity in Drosophila. PLoS One 7: e47452.
66. Lejeune FX, Mesrob L, Parmentier F, Bicep C, Vazquez-Manrique RP, et al. (2012) Large-scale functional RNAi screen in C. elegans identifies genes that regulate the dysfunction of mutant polyglutamine neurons. BMC Genomics 13: 91.
67. Carninci P, Kasukawa T, Katayama S, Gough J, Frith MC, et al. (2005) The transcriptional landscape of the mammalian genome (The FANTOM Consortium). Science 309: 1559–1563.
68. Yamanaka T, Horikoshi Y, Izumi N, Suzuki A, Mizuno K, et al. (2006) Lgl mediates apical domain disassembly by suppressing the PAR-3-aPKC-PAR-6 complex to orient apical membrane polarity. J Cell Sci 119: 2107–2118.

Neurobiology of Disease 74 (2015) 25–31

Contents lists available at ScienceDirect

Neurobiology of Disease

journal homepage: www.elsevier.com/locate/ynbdi

Sigma-1 receptor is involved in degradation of intranuclear inclusions in a cellular model of Huntington's disease

Yasuo Miki *, Kunikazu Tanji, Fumiaki Mori, Koichi Wakabayashi

Department of Neuropathology, Institute of Brain Science, Hirosaki University Graduate School of Medicine, 5 Zaifu-cho, Hirosaki, Japan

ARTICLE INFO

Article history:
Received 10 September 2014
Accepted 4 November 2014
Available online 14 November 2014

Keywords:
Sigma-1 receptor
Huntington's disease
Neuronal nuclear inclusions
Ubiquitin–proteasome system
Endoplasmic reticulum chaperone
Endoplasmic reticulum-associated degradation

ABSTRACT

The sigma-1 receptor (SIGMAR1) is one of the endoplasmic reticulum (ER) chaperones, which participate in the degradation of misfolded proteins via the ER-related degradation machinery linked to the ubiquitin–proteasome pathway. ER dysfunction in the formation of inclusion bodies in various neurodegenerative diseases has also become evident. Recently, we demonstrated that accumulation of SIGMAR1 was common to neuronal nuclear inclusions in polyglutamine diseases including Huntington's disease. Our study also indicated that SIGMAR1 might shuttle between the cytoplasm and the nucleus. In the present study, we investigated the role of SIGMAR1 in nuclear inclusion (NI) formation, using HeLa cells transfected with N-terminal mutant huntingtin. Cell harboring the mutant huntingtin produced SIGMAR1-positive NIs. SIGMAR1 siRNA and a specific inhibitor of the proteasome (epoxomicin) caused significant accumulation of aggregates in the cytoplasm and nucleus. A specific inhibitor of exportin 1 (leptomycin B) also caused NIs. Huntingtin became insolubilized in Western blot analysis after treatments with SIGMAR1 siRNA and epoxomicin. Furthermore, proteasome activity increased chronologically along with the accumulation of mutant huntingtin, but was significantly reduced in cells transfected with SIGMAR1 siRNA. By contrast, overexpression of SIGMAR1 reduced the accumulation of NIs containing mutant huntingtin. Although the LC3-I level was decreased in cells treated with both SIGMAR1 siRNA and control siRNA, the levels of LC3-II and p62 were unchanged. SIGMAR1 agonist and antagonist had no effect on cellular viability and proteasome activity. These findings suggest that the ubiquitin–proteasome pathway is implicated in NI formation, and that SIGMAR1 degrades aberrant proteins in the nucleus via the ER-related degradation machinery. SIGMAR1 might be a promising candidate for therapy of Huntington's disease.

Introduction

Huntington's disease (HD) is an autosomal dominant neurodegenerative disease manifested classically as progressive chorea and psychiatric symptoms, resulting in severe dementia (Huntington, 1872). HD is now known to be one of the nine polyglutamine diseases caused by the expansion of trinucleotide repeats encoding polyglutamine in their causative genes (Orr et al., 1993; Kawaguchi et al., 1994; Koide et al., 1994; Nagafuchi et al., 1994; Pulst et al., 1996; Martindale et al., 1998). Accumulation of misfolded proteins in proteinaceous inclusions is considered to be a common feature of many neurodegenerative diseases, and clearance of abnormal proteins by the ubiquitin–proteasome system (UPS) and/or autophagy-lysosome system is paramount for cellular survival. In HD, neuronal nuclear inclusions (NNIs) containing mutant huntingtin protein is a pathological hallmark (Sapp et al., 1997). The accumulation of mutant huntingtin in neurons impairs mediators of promoter accessibility (TATA box-binding protein, TAFII130, and specificity protein I), neurotransmitter release at presynaptic nerve terminals, and mitochondrial function (Dunah et al., 2002; Schaffar et al., 2004; Zhai et al., 2005; Huang et al., 2011; Mochel and Haller, 2011). Furthermore, mutant huntingtin has adverse effects on various protein degradation pathways, such as impairment of UPS, engulfment of cytosolic cargo by autophagosomes, and gp78, an endoplasmic reticulum (ER) membrane-anchored ubiquitin ligase (E3) involved in ER-associated protein degradation (ERAD) (Bennett et al., 2007; Martinez-Vicente et al., 2010; Yang et al., 2010). However, it remains to be elucidated how aberrant proteins in the nucleus are degraded in HD.

The sigma-1 receptor (SIGMAR1), encoded by the SIGMAR1 gene, is a non-opioid ER protein with a molecular mass of 24 kDa (Martin et al., 1976; Quirion et al., 1992; Kekuda et al., 1996; Hayashi et al., 2011). In addition to the regulation of ion channels, synaptogenesis, and neuronal plasticity, SIGMAR1 functions as a molecular chaperone in the ER. ER chaperones not only facilitate the proper folding of newly synthesized proteins, but also prevent the accumulation of misfolded proteins by consigning them to ERAD, suggesting that SIGMAR1 also contributes

* Corresponding author at: Department of Neuropathology, Institute of Brain Science, Hirosaki University Graduate School of Medicine, 5 Zaifu-cho, Hirosaki 036-8562, Japan. Fax: +81 172 39 5132.
E-mail address: yasuomiki@hotmail.com (Y. Miki).
Available online on ScienceDirect (www.sciencedirect.com).

http://dx.doi.org/10.1016/j.nbd.2014.11.005
0969-9961/© 2014 Elsevier Inc. All rights reserved.

to cellular survival (Hayashi et al., 2011; Schröder and Kaufman, 2005). We recently demonstrated that the accumulation of SIGMAR1 was common to NNIs in the brains of patients with five polyglutamine diseases (HD, dentatorubral-pallidoluysian atrophy, and spinocerebellar ataxia types 1–3) and intranuclear inclusion body disease (Miki et al., 2014). Double-immunocytofluorescence and Western blot analyses of cultured cells demonstrated that a specific exportin 1 inhibitor (leptomycin B) sequestered SIGMAR1 within the nucleus, acting together with p62, and that furthermore, an ER stressor (thapsigargin) caused migration of SIGMAR1 in the nucleus. These findings indicate that SIGMAR1 might shuttle between the cytoplasm and the nucleus, potentially associated with NNI clearance via ERAD (Miki et al., 2014).

We hypothesized that if expanded polyglutamine in the ER or the nucleus is cleared through ERAD, blocking a putative pathway of SIGMAR1 would provide similar pathological kinetics in NNI formation. In the present study, immunocytofluorescence, Western blot analysis, and proteasome activity assay of a cellular model of HD were performed to better understand the involvement of SIGMAR1 in the degradation of abnormal proteins in NNIs through ERAD. Our results indicated that abnormal proteins in the nucleus might be degraded by UPS through ERAD, suggesting that modulation of SIGMAR1 could have potential therapeutic applications for HD.

Material and methods

Cell culture and transfection

HeLa cells were purchased from the Japanese Collection of Research Bioresources Cell Bank (Osaka, Japan), and maintained in Dulbecco's modified Eagle medium supplemented with 10% fetal calf serum and antibiotics.

siRNA-mediated knockdown

siRNA was purchased from Thermo Fisher Scientific (Waltham, MA, USA). siRNA at a final concentration of 20 μM for SIGMAR1 (5′-GAAUGC GGGUGGCUGGAUG-3′, 5′-GGCUUGAGCUCACCACCUA-3′, 5′-GAGCUG GCCUUCUCUCGUC-3′, and 5′-CCAAACACAUGGAUGGUGG-3′) and non-targeting controls (D-001810-10-20) were transfected into cultured cells using siRNAMAX (Invitrogen, Carlsbad, USA).

SIGMAR1 overexpression

An expression clone of SIGMAR1 cDNA was purchased from Gene Copoeia (Rockville, Maryland, USA) and transfected into cultured cells using Fugene® 6 (Roche, Basel, Switzerland).

Antibodies and reagents

Goat polyclonal anti-SIGMAR1 (Santa Cruz Biotechnology, Dallas, TX), mouse monoclonal anti-p62 (BD Transduction Laboratories, San Jose, CA), mouse monoclonal anti-ubiquitin (FK1; Millipore, Bedford, NJ), rabbit polyclonal anti-microtubule-associated protein 1 light chain 3 (LC3; Sigma, St. Louis, MO), goat polyclonal anti-Bip (GRP78; Santa Cruz Biotechnology), rabbit polyclonal anti-β-actin (Sigma), and rabbit monoclonal anti-GFP antibody (Life Technologies, Carlsbad, USA) were used as primary antibodies. In addition, rabbit polyclonal anti-PML (Medical and Biological Laboratories, Nagoya, Japan), anti-Coilin (Santa Cruz Biotechnology) and anti-PSPC1 antibodies (Sigma) were also used for the detection of nuclear bodies including PML bodies, Cajal bodies, and paraspeckles, respectively (Wang et al., 2002; Spector, 2006). To investigate the role of SIGMAR1 in NNI formation, a SIGMAR1 agonist (PRE-084; Sigma), a SIGMAR1 antagonist (BD1063; Sigma), and specific inhibitors of the proteasome (epoxomicin; Peptide institute, Osaka, Japan) and exportin 1 (leptomycin B; Sigma) were utilized (Kudo et al., 1999; Meng et al., 1999; Amer et al., 2013; Hyrskyluoto et al., 2013).

Immunocytochemistry and semi-quantitative analysis

HeLa cells were treated with siRNA-SIGMAR1, epoxomicin, leptomycin B, PRE-084, and BD1063 at a final concentration of 20 μM, 20 μM, 0.1 μM, 10 nM, 0.3 μM, and 50 μM, respectively (Kudo et al., 1999; Meng et al., 1999; Amer et al., 2013; Hyrskyluoto et al., 2013). The cells were then transfected for 24 h with 1 μg of GFP-tagged plasmid DNA containing a normal (Q23; Addgene, Cambridge, MA; plasmid 40263) or pathological CAG-repeat length (Q74; Addgene; plasmid 40262) of the huntingtin exon 1 (Narain et al., 1999). The SIGMAR1 gene was also overexpressed in the cells transfected with Q74 and examined at after 12, 24, and 36 h. For double-immunostaining, the cells were fixed with 4% paraformaldehyde, and permeabilized with 0.1% Triton X-100 for 10 min, followed by incubation with anti-SIGMAR1 (1:200), anti-ubiquitin (1:400), anti-PML (1:400), anti-Coilin (1:100), and anti-PSPC1 (1:500) antibodies. Alexa Fluor 488- and 594-conjugated secondary antibodies (Invitrogen) were utilized as secondary antibodies. After a rinse in phosphate-buffered saline (PBS), the cells were mounted and examined as described above. In order to count the nuclear inclusions in cells with each treatment, semi-quantitative analysis was performed based on 10 randomly chosen low-power fields.

Western blot analysis

After transfection with siRNA-SIGMAR1, siRNA-control, and SIGMAR1 or treatment with epoxomicin, leptomycin B, PRE-084, and BD1063, HeLa cells were transfected with Q74 for 24 h as described above, then harvested to assess the expression levels in the total lysates. The cells were lysed with sample buffer [75 mM Tris–HCl, pH 6.8, 4% sodium dodecyl sulfate (SDS), 25% glycerol, 5% β-mercaptoethanol]. Western blot analysis was performed as reported previously (Zhang et al., 2008). Anti-SIGMAR1 (1:200), anti-GFP (1:2000), anti-β-actin (1:3000), anti-p62 (1:100), and anti-LC3 (1:4000) were used as the primary antibodies. Horseradish peroxidase-conjugated anti-goat, anti-mouse, and anti-rabbit IgG (Santa Cruz Biotechnology) were used as the secondary antibodies.

Proteasomal activity assay

Chymotryptic, tryptic, and caspase proteasome activities were measured as described previously with minor modifications (Lee et al., 2010). HeLa cells were washed with PBS and pelleted by centrifugation. The cell pellets were sonicated in homogenization buffer [25 mM Tris, pH 7.5, 100 mM NaCl, 5 mM ATP, 0.2% (v/v) NP-40 and 20% glycerol], and cell debris was removed by centrifugation at 4 °C. Protein concentration in the resulting crude cellular extracts was determined by the bicinchoninic acid method (Pierce, Rockford, IL). One hundred micrograms of protein from crude cellular extracts of each sample was diluted with buffer I [50 mM Tris–HCl, pH 7.4, 2 mM dithiothreitol, 5 mM $MgCl_2$, 2 mM ATP] to a final volume of 0.5 mL (assayed in quadruplicate). Fluorogenic proteasome substrates were purchased from Boston Biochem (Cambridge, MA): Suc-LLVY-7-amido-4-methylcoumarin (AMC) (chymotrypsin-like peptidase activity), Z-ARR-AMC (trypsin-like peptidase activity), and Z-LLE-AMC (caspase-like or peptidylglutamyl peptide-hydrolyzing activity). Each was dissolved in DMSO and brought to a final concentration of 80 μM. Proteolytic activities were assessed in 2 h at 37 °C by measuring the release of the fluorescent group AMC using a fluorescence plate reader (Fluoroskan Ascent; Thermo Scientific, Waltham, MA) with excitation and emission wavelengths of 380 and 460 nm, respectively.

Quantification and statistics

Statistical analyses were performed using two-sample t test and one-way ANOVA. Differences were considered statistically significant at $P < 0.05$.

Results

SIGMAR1 immunoreactivity in HeLa cells transfected with either the normal or pathological huntingtin gene

We first transfected HeLa cells with GFP-labeled huntingtin bearing either the Q23 or the Q74 repeat, and found that only Q74-transfected HeLa cells formed nuclear and cytoplasmic aggregates of the huntingtin protein (Fig. 1A). The anti-SIGMAR1 antibody immunostained most of the small intranuclear mutant huntingtin aggregates (Figs. 1B,C). Some of the SIGMAR1-immunopositive nuclear inclusions were also immunolabeled with anti-ubiquitin (Figs. 1D–F). Cytoplasmic inclusions were SIGMAR1-negative. Because mutant huntingtin is known to be co-localized with nuclear bodies and negatively regulates transcription and splicing (Busch et al., 2003), we further immunolabeled the intranuclear SIGMAR1-positive structures with antibodies against nuclear bodies, including PML bodies, Cajal bodies, and paraspeckles. Only anti-PML antibody stained some of the SIGMAR1-positive nuclear inclusions (Figs. 1G–I).

Semi-quantitative analysis of intranuclear aggregates

To investigate whether or not blocking a SIGMAR1-associated putative degradation pathway would cause NNI formation, we treated mutant huntingtin-induced cells with SIGMAR1 siRNA, leptomycin B, and epoxomicin, and performed semi-quantitative analysis. Both SIGMAR1 siRNA and epoxomicin significantly increased the amount of mutant huntingtin aggregates in both the cytoplasm and nucleus (Figs. 2A,B). In addition, leptomycin B doubled the amount of mutant huntingtin aggregates in the nucleus (Fig. 2C).

Western blot analysis and proteasome activity assay

Immunoblotting demonstrated that treatment of mutant huntingtin-induced cells with both SIGMAR1 siRNA and epoxomicin caused the appearance of high-molecular-mass GFP expression bands at about 100 kDa, whereas no high-molecular-mass mutant huntingtin was found without SIGMAR1 siRNA treatment (Fig. 2D). PRE-084 and BD1063 did not affect the level of GFP expression (data not shown).

We performed a proteasome activity assay of mutant huntingtin-induced cells treated with PRE-084, BD1063, SIGMAR1 siRNA, and control siRNA. In the cells transfected with SIGMAR1 siRNA, proteasome activity was significantly reduced in two out of the three UPS substrates, compared with control cells and cells with control siRNA (Fig. 3). No significant change in proteasome activity was observed in cells treated with PRE-084 and BD1063.

We also performed immunoblotting of LC3, an autophagy–lysosome system marker, and p62, a substrate of the autophagy–lysosome system. Compared with untreated HeLa cells, mutant huntingtin induction increased the expression of LC3-II. However, with or without mutant huntingtin gene induction, SIGMAR1 silencing increased the level of LC3-II relative to that of LC3-I, whereas the level of p62 was unchanged (Fig. 4).

SIGMAR1 overexpression

To further confirm the involvement of SIGMAR1 in nuclear inclusion formation, HeLa cells were transfected with 0.5 μg, 1.0 μg, and 1.5 μg of expression plasmid DNA containing SIGMAR1. Each group successfully expressed FLAG-tagged SIGMAR1. Overexpression of more than 1.0 μg of SIGMAR1 clearly caused cellular toxicity along with expression of Bip, a marker of ER stress (Supplementary material). Therefore, transfection with 0.25 μg SIGMAR1 was chosen, and overexpression was performed in huntingtin-induced cells. Mutant huntingtin was expressed in cells with or without SIGMAR1 overexpression (Figs. 5A,D). Mutant huntingtin-induced cells formed cytoplasmic and nuclear aggregates over time (Figs. 5B,C). On the other hand, SIGMAR1 overexpression clearly prevented aggregate formation (Figs. 5E,F,G).

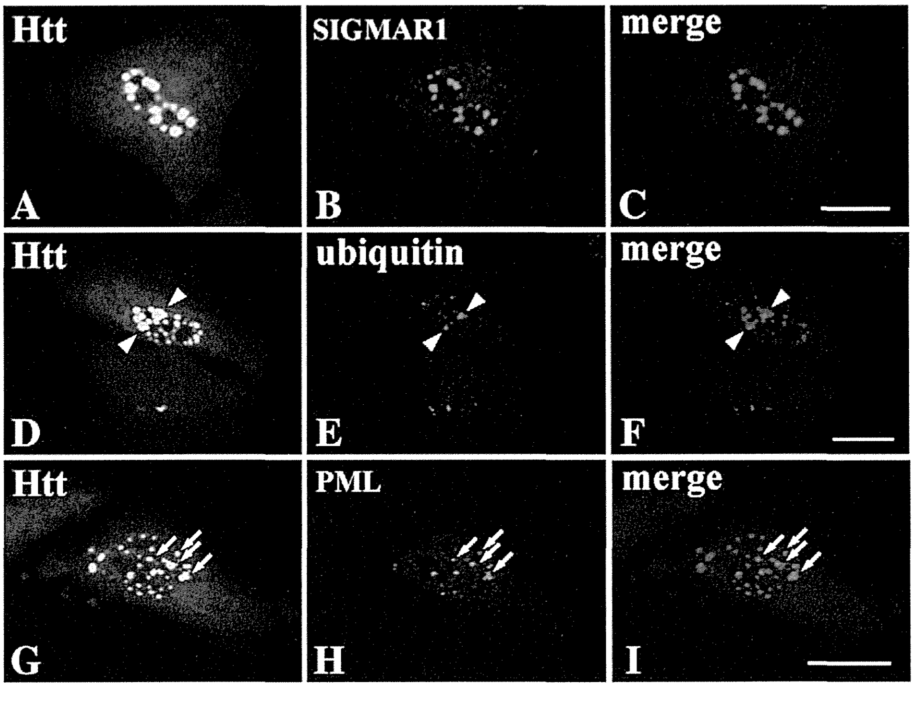

Fig. 1. Intranuclear protein aggregates in a cellular model of Huntington's disease. (A, D, G) Aggregation of mutant huntingtin (Htt) in the nucleus. (B, C) Co-localization of Htt with SIGMAR1. (E, F) Partial co-localization of ubiquitin and Htt (arrowheads). (H, I) Partial co-localization of PML and Htt (arrows). Bars = 20 μm.

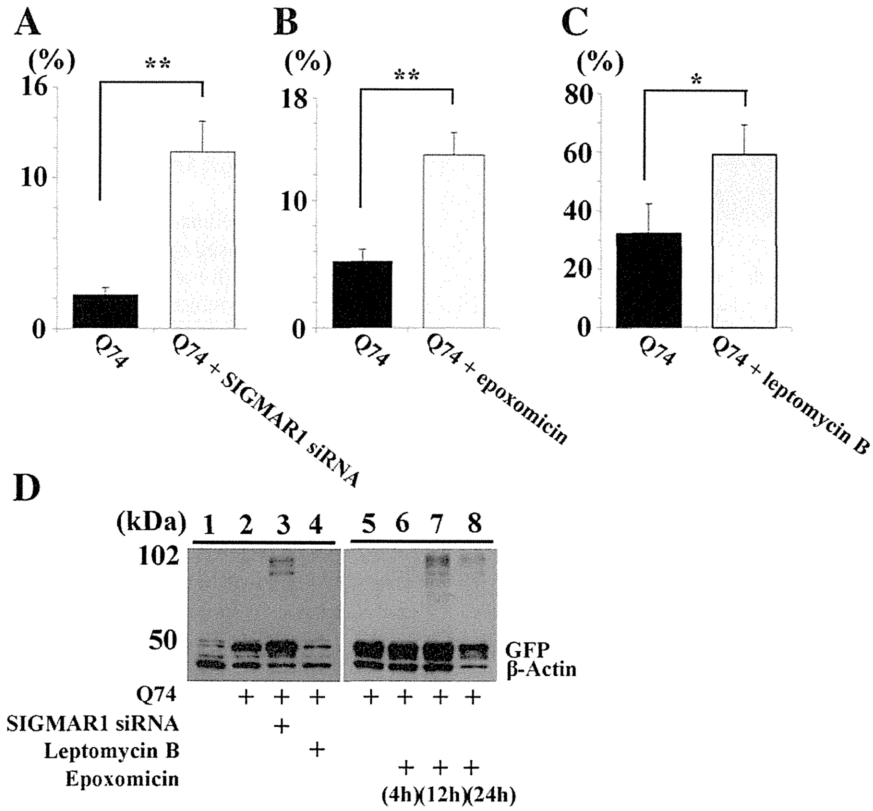

Fig. 2. Increased number of mutant huntingtin aggregates after treatments with SIGMAR1 siRNA and specific inhibitors for proteasome (epoxomicin) and exportin 1 (leptomycin B). (A, B) Increased number of nuclear aggregates after treatments with SIGMAR1 siRNA (A) and epoxomicin (B). (C) Increased number of nuclear aggregates after treatment with leptomycin B. (D) High-molecular-mass GFP-tagged mutant Htt caused by treatment with SIGMAR1 siRNA (lane 3) and epoxomicin (lane 7). $^*P < 0.05$, $^{**}P < 0.01$.

Time course analysis of proteasome activities in mutant huntingtin-induced cells showed that proteasome activity increased chronologically in accordance with the accumulation of mutant huntingtin. Accordingly, proteasome activity in SIGMAR1-overexpressing cells was significantly lower than that in controls (Fig. 6).

Discussion

In the present study, SIGMAR1 was predominantly incorporated in small intranuclear mutant huntingtin aggregates, some of which were ubiquitinated. The SIGMAR1-immunopositive nuclear inclusions were

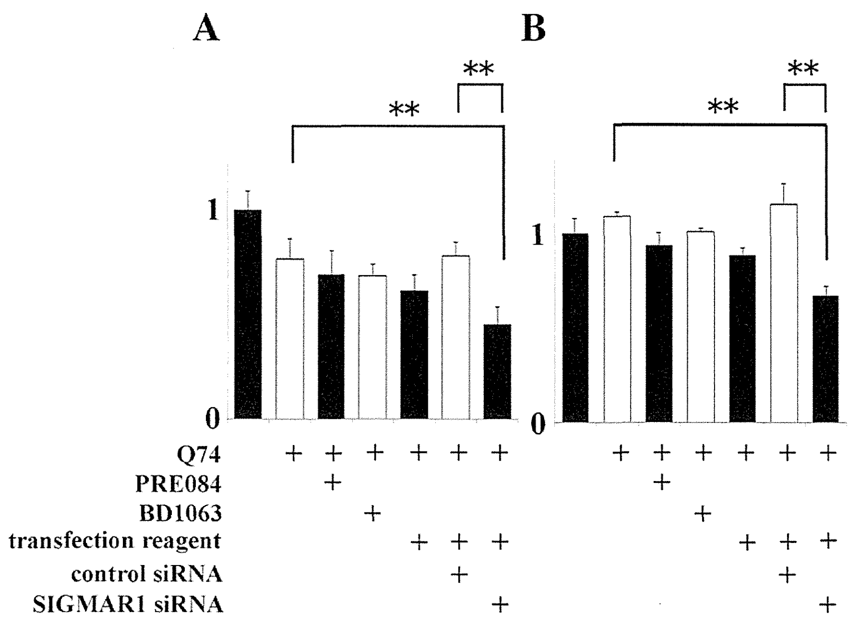

Fig. 3. Proteasomal activity of SIGMAR1 agonist (PRE-084) and antagonist (BD1063), and siRNA. Compared with controls (lanes 2 and 6 in A and B), there was a significant decrease of proteasome activity in mutant huntingtin-induced cells transfected with SIGMAR1 siRNA (lane 7 in A and B). No significant changes in proteasomal activity were evident between controls and PRE-084- or BD1063-treated cells (lanes 2–5 in A and B). Chymotrypsin-like activity in A: Z-ARR; B: Suc-LLVY.

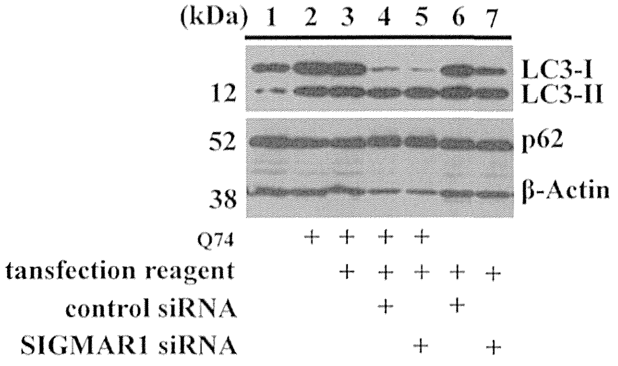

Fig. 4. Expression levels of autophagosomal proteins in mutant huntingtin-induced cells. Although the LC3-I level is decreased (lanes 4 and 5), the levels of autophagy substrate (p62 and LC3-II) are similar between controls and SIGMAR1 siRNA-treated HeLa cells (lanes 4–7).

also partially PML-positive. PML bodies are suggested to play a role in transcriptional regulation and nuclear protein sequestration (Spector, 2006). PML bodies recruit the UPS component and promote their degradation by UPS. Coalescence of small bodies into larger ones has also been shown (Lafarga et al., 2002; Janer et al., 2006; Spector, 2006). Although our previous study showed that large NNIs were strongly positive for SIGMAR1 in human brains affected by polyglutamine diseases and intranuclear inclusion body disease (Miki et al., 2014), the small SIGMAR1-positive nuclear inclusions observed in the present study might also be a target for UPS and represent an early stage of protein aggregation.

In the present cellular model of HD, silencing of SIGMAR1 function significantly increased the number of nuclear inclusions and caused accumulation of high-molecular-mass GFP-labeled mutant huntingtin, as shown by Western blot analysis. These phenomena were reproduced by treatment with a specific proteasome inhibitor, epoxomicin. Leptomycin B increased the number of intranuclear, but not cytoplasmic, aggregates. Proteasome activity was significantly lower in cells transfected with SIGMAR1 siRNA. SIGMAR1 is one of the ER chaperones associated with ERAD and is considered to shuttle between the nucleus and the cytoplasm (Miki et al., 2014). These findings suggest that SIGMAR1 might be intrinsically involved in the degradation of mutant huntingtin in the nucleus through ERAD.

ER homeostasis can be disrupted in various neurodegenerative disorders including polyglutamine diseases, α-synucleinopathy, TDP-43 proteinopathy and tauopathy (Roussel et al., 2013). Mutant huntingtin

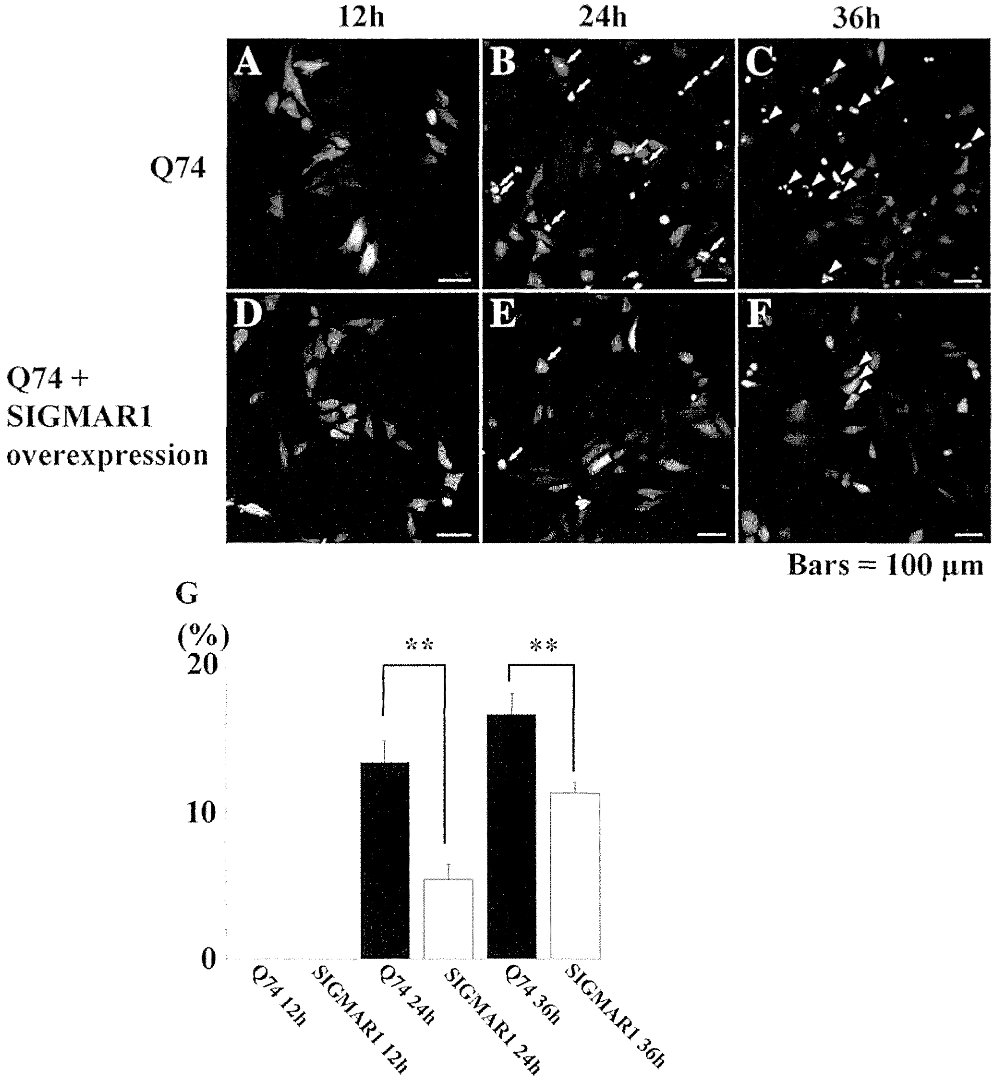

Fig. 5. Effect of SIGMAR1 overexpression on aggregate formation in mutant huntingtin-induced cells. (A, D) Expression of GFP-tagged mutant huntingtin in controls (A) and cells overexpressing SIGMAR1 (D). (B, E) Formation of mutant huntingtin aggregates in the cytoplasm and nucleus over time (B: arrows; E: arrowheads). (C, F) Prevention of mutant huntingtin aggregate formation by SIGMAR1 overexpression (C: arrows; F: arrowheads). (G) Semi-quantitative analysis showing significant reduction of mutant huntingtin aggregates in cells overexpressing SIGMAR1. Bars = 100 μm, **P < 0.01.

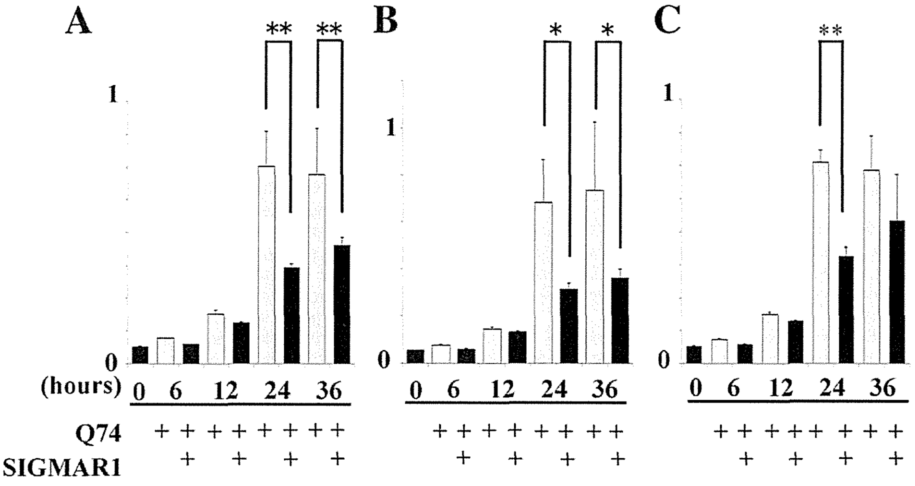

Fig. 6. Time series analysis of proteasomal activity in cells overexpressing SIGMAR1. Chymotryptic (A), tryptic (B) and caspase proteasome activities (C) gradually increased in mutant huntingtin-induced cells. Proteasomal activity was significantly lower in cells with overexpressing SIGMAR1 for 24 and 36 h in A (Suc-LLVY) and B (Z-ARR) and for 24 h in C (Z-LLE). $^{*}P < 0.05$, $^{**}P < 0.01$.

induces ER stress, and ERAD is impaired even at an early stage of HD (Duennwald and Lindquist, 2008). Recent studies have shown that the soluble form of poly-expanded huntingtin, rather than large aggregates, is toxic and causes ER stress, and that the ERAD substrate accumulates even before visible development of huntingtin aggregates, induction of ER stress markers correlating with the increase in the latter (Leitman et al., 2013). In the present study, SIGMAR1 overexpression prevented the formation of mutant huntingtin aggregates along with the reduction of proteasome activity. These findings imply that mutant huntingtin protein might be cleared upon overexpression of SIGMAR1. Thus, SIGMAR1 might act even from an early phase of HD. We were unable to find any period of increased proteasome activity in cells that overexpressed SIGMAR1. SIGMAR1 has multiple functions as an ER chaperone. Further investigations should be done to clarify whether proteasome activity is increased at the very early phase of SIGMAR1 transfection, or whether other SIGMAR1 functions, such as refolding of abnormal proteins, might contribute to clearance of mutant huntingtin.

Mori et al. (2012) demonstrated that autophagy-specific proteins (LC3 and NBR1) were not incorporated into NNIs in brains affected by polyglutamine diseases. HDAC6, an enzyme essential for aggresome formation, was recruited into cytoplasmic huntingtin aggregates, but was not associated with NNI formation (Iwata et al., 2005; Miki et al., 2011). In mutant huntingtin-induced cells, the macroautophagy substrate was not correlated with any increase in autophagy-mediated degradation. Iwata et al. (2009) further reported that nuclear ubiquitin ligase San1p and UHRF-2 accelerated the clearance of nuclear polyglutamine aggregates. Thus, the principal pathway for clearance of abnormal protein might differ between the inside and the outside of the nucleus. In the present study, the observed increase in LC3-II relative to LC3-I after transfection with SIGMAR1 siRNA suggested either up-regulation of autophagosome formation or blockage of autophagic degradation. However, the levels of LC3-II and p62 expression were similar in both of the groups transfected with SIGMAR1 siRNA and control siRNA. Proteasome activity increased chronologically in parallel with the accumulation of mutant huntingtin. Although the decreased level of LC3-I expression in huntingtin-induced cells transfected with SIGMAR1 siRNA may indicate strong cellular toxicity, autophagy influx appeared to increase in order to compensate for UPS. Autophagy might be ineffective for clearance of nuclear aggregates, and UPS may be primarily associated with NNI formation.

Several SIGMAR1 agonists are available. Some have been used clinically as antidepressants, e.g., Opipramol and Fluvoxamine, which are known to possess affinity for SIGMAR1. Indeed, PRE-084 improves the survival of cells bearing mutant huntingtin by activation of NF-κB (Hyrskyluoto et al., 2013). In the present study, PRE-084 and BD1063 did not affect aggregate formation or proteasome activity, indicating that these drugs might not be directly associated with abnormal protein degradation. Our study clearly showed that SIGMAR1 might play a pivotal role in NNI clearance. SIGMAR1 agonists involved in the potential protein degradation pathway of the nucleus, such as those with proteasome activity, may have potential therapeutic value for HD.

In conclusion, our present findings strongly suggest that SIGMAR1 is deeply involved in the clearance of abnormal proteins in NNIs through ERAD. Activation of SIGMAR1 might lead to reduction of mutant huntingtin toxicity.

Supplementary data to this article can be found online at http://dx.doi.org/10.1016/j.nbd.2014.11.005.

Acknowledgment

This work was supported by JSPS KAKENHI Grant Numbers 26860655 (Y.M.), 26430050 (K.T.), 26430049 (F.M.) and 24300131 (K.W.), Hirosaki University Grant for Exploratory Research by Young Scientists (Y.M.), a Grant for Hirosaki University Institutional Research (K.W.) and the Research Committee for Ataxic Disease (K.W.) from the Ministry of Health, Labour and Welfare, Japan.

References

Amer, M.S., McKeown, L., Tumova, S., et al., 2013. Inhibition of endothelial cell Ca^{2+} entry and transient receptor potential channels by sigma-1 receptor ligands. Br. J. Pharmacol. 168, 1445–1455.
Bennett, E.J., Shaler, T.A., Woodman, B., et al., 2007. Global changes to the ubiquitin system in Huntington's disease. Nature 448, 704–708.
Busch, A., Engemann, S., Lurz, R., et al., 2003. Mutant huntingtin promotes the fibrillogenesis of wild-type huntingtin: a potential mechanism for loss of huntingtin function in Huntington's disease. J. Biol. Chem. 278, 41452–41461.
Duennwald, M.L., Lindquist, S., 2008. Impaired ERAD and ER stress are early and specific events in polyglutamine toxicity. Genes Dev. 22, 3308–3319.
Dunah, A.W., Jeong, H., Griffin, A., et al., 2002. Sp1 and TAFII130 transcriptional activity disrupted in early Huntington's disease. Science 296, 2238–2243.
Hayashi, T., Tsai, S.Y., Mori, T., et al., 2011. Targeting ligand-operated chaperone sigma-1 receptors in the treatment of neuropsychiatric disorders. Expert Opin. Ther. Targets 15, 557–577.
Huang, S., Ling, J.J., Yang, S., et al., 2011. Neuronal expression of TATA box-binding protein containing expanded polyglutamine in knock-in mice reduces chaperone protein response by impairing the function of nuclear factor-Y transcription factor. Brain 134, 1943–1958.
Huntington, G., 1872. On chorea. Med. Surg. Rep. Phila. 26, 317–321.
Hyrskyluoto, A., Pulli, I., Törnqvist, K., et al., 2013. Sigma-1 receptor agonist PRE084 is protective against mutant huntingtin-induced cell degeneration: involvement of calpastatin and the NF-κB pathway. Cell Death Dis. 4, e646.
Iwata, A., Riley, B.E., Johnston, J.A., et al., 2005. HDAC6 and microtubules are required for autophagic degradation of aggregated huntingtin. J Biol Chem. 280, 40282–40292.

Iwata, A., Nagashima, Y., Matsumoto, L., et al., 2009. Intranuclear degradation of polyglutamine aggregates by the ubiquitin–proteasome system. J. Biol. Chem. 284, 9796–9803.
Janer, A., Martin, E., Muriel, M.P., et al., 2006. PML clastosomes prevent nuclear accumulation of mutant ataxin-7 and other polyglutamine proteins. J. Cell Biol. 174, 65–76.
Kawaguchi, Y., Okamoto, T., Taniwaki, M., et al., 1994. CAG expansions in a novel gene for Machado–Joseph disease at chromosome 14q32.1. Nat. Genet. 8, 221–228.
Kekuda, R., Prasad, P.D., Fei, Y.J., et al., 1996. Cloning and functional expression of the human type 1 sigma receptor (hSigmaR1). Biochem. Biophys. Res. Commun. 229, 553–558.
Koide, R., Ikeuchi, T., Onodera, O., et al., 1994. Unstable expansion of CAG repeat in hereditary dentatorubralpallidoluysianatrophy (DRPLA). Nat. Genet. 6, 9–13.
Kudo, N., Matsumori, N., Taoka, H., et al., 1999. Leptomycin B inactivates CRM1/exportin 1 by covalent modification at a cysteine residue in the central conserved region. Proc. Natl. Acad. Sci. U. S. A. 96, 9112–9117.
Lafarga, M., Berciano, M.T., Pena, E., et al., 2002. Clastosome: a subtype of nuclear body enriched in 19S and 20S proteasomes, ubiquitin, and protein substrates of proteasome. Mol. Biol. Cell 13, 2771–2782.
Lee, B.H., Lee, M.J., Park, S., et al., 2010. Enhancement of proteasome activity by a small-molecule inhibitor of USP14. Nature 467, 179–184.
Leitman, J., Ulrich Hartl, F., Lederkremer, G.Z., 2013. Soluble forms of polyQ-expanded huntingtin rather than large aggregates cause endoplasmic reticulum stress. Nat. Commun. 4, 2753.
Martin, W.R., Eades, C.G., Thompson, J.A., et al., 1976. The effects of morphine- and nalorphine-like drugs in the nondependent and morphine-dependent chronic spinal dog. J. Pharmacol. Exp. Ther. 197, 517–532.
Martindale, D., Hackam, A., Wieczorek, A., et al., 1998. Length of huntingtin and its polyglutamine tract influences localization and frequency of intracellular aggregates. Nat. Genet. 18, 150–154.
Martinez-Vicente, M., Talloczy, Z., Wong, E., et al., 2010. Cargo recognition failure is responsible for inefficient autophagy in Huntington's disease. Nat. Neurosci. 13, 567–576.
Meng, L., Mohan, R., Kwok, B.H., et al., 1999. Epoxomicin, a potent and selective proteasome inhibitor, exhibits in vivo antiinflammatory activity. Proc. Natl. Acad. Sci. U. S. A. 96, 10403–10408.
Miki, Y., Mori, F., Tanji, K., et al., 2011. Accumulation of histone deacetylase 6, an aggresome-related protein, is specific to Lewy bodies and glial cytoplasmic inclusions. Neuropathology 31, 561–568.
Miki, Y., Mori, F., Kon, T., et al., 2014. Accumulation of the sigma-1 receptor is common to neuronal nuclear inclusions in various neurodegenerative diseases. Neuropathology 34, 148–158.
Mochel, F., Haller, R.G., 2011. Energy deficit in Huntington disease: why it matters. J. Clin. Invest. 121, 493–499.
Mori, F., Tanji, K., Odagiri, S., et al., 2012. Autophagy-related proteins (p62, NBR1 and LC3) in intranuclear inclusions in neurodegenerative diseases. Neurosci. Lett. 522, 134–138.
Nagafuchi, S., Yanagisawa, H., Sato, K., et al., 1994. Dentatorubral and pallidoluysian atrophy expansion of an unstable CAG trinucleotide on chromosome 12p. Nat. Genet. 6, 14–18.
Narain, Y., Wyttenbach, A., Rankin, J., et al., 1999. A molecular investigation of true dominance in Huntington's disease. J. Med. Genet. 36, 739–746.
Orr, H.T., Chung, M.Y., Banfi, S., et al., 1993. Expansion of an unstable trinucleotide CAG repeat in spinocerebellar ataxia type 1. Nat. Genet. 4, 221–226.
Pulst, S.M., Nechiporuk, A., Nechiporuk, T., et al., 1996. Moderate expansion of a normally biallelic trinucleotide repeat in spinocerebellar ataxia type 2. Nat. Genet. 14, 269–276.
Quirion, R., Bowen, W.D., Itzhak, Y., et al., 1992. A proposal for the classification of sigma binding sites. Trends Pharmacol. Sci. 13, 85–86.
Roussel, B.D., Kruppa, A.J., Miranda, E., et al., 2013. Endoplasmic reticulum dysfunction in neurological disease. Lancet Neurol. 12, 105–118.
Sapp, E., Schwarz, C., Chase, K., et al., 1997. Huntingtin localization in brains of normal and Huntington's disease patients. Ann. Neurol. 42, 604–612.
Schaffar, G., Breuer, P., Boteva, R., et al., 2004. Cellular toxicity of polyglutamine expansion proteins: mechanism of transcription factor deactivation. Mol. Cell 15, 95–105.
Schröder, M., Kaufman, R.J., 2005. The mammalian unfolded protein response. Annu. Rev. Biochem. 74, 739–789.
Spector, D.L., 2006. SnapShot: cellular bodies. Cell 127, 1071.
Wang, I.F., Reddy, N.M., Shen, C.K., 2002. Higher order arrangement of the eukaryotic nuclear bodies. Proc. Natl. Acad. Sci. U. S. A. 99, 13583–13588.
Yang, H., Liu, C., Zhong, Y., et al., 2010. Huntingtin interacts with the cue domain of gp78 and inhibits gp78 binding to ubiquitin and p97/VCP. PLoS One 5, e8905.
Zhai, W., Jeong, H., Cui, L., et al., 2005. In vitro analysis of huntingtin-mediated transcriptional repression reveals multiple transcription factor targets. Cell 123, 1241–1253.
Zhang, H.X., Tanji, K., Mori, F., et al., 2008. Epitope mapping of 2E2-D3, a monoclonal antibody directed against human TDP-43. Neurosci. Lett. 434, 170–174.

Wakabayashi et al. Acta Neuropathologica Communications 2014, 2:173
http://www.actaneurocomms.org/content/2/1/173

ACTA NEUROPATHOLOGICA COMMUNICATIONS

RESEARCH Open Access

Analysis of microRNA from archived formalin-fixed paraffin-embedded specimens of amyotrophic lateral sclerosis

Koichi Wakabayashi[1*], Fumiaki Mori[1], Akiyoshi Kakita[2], Hitoshi Takahashi[3], Jun Utsumi[4] and Hidenao Sasaki[4]

Abstract

Background: MicroRNAs (miRNAs) are noncoding small RNAs that regulate gene expression. This study investigated whether formalin-fixed paraffin-embedded (FFPE) specimens from postmortem cases of neurodegenerative disorders would be suitable for miRNA profiling.

Results: Ten FFPE samples from 6 cases of amyotrophic lateral sclerosis (ALS) and 4 neurologically normal controls were selected for miRNA analysis on the basis of the following criteria for RNA quality: (i) a postmortem interval of less than 6 hours, (ii) a formalin fixation time of less than 4 weeks, (iii) an RNA yield per sample of more than 500 ng, and (iv) sufficient quality of the RNA agarose gel image. An overall RNA extraction success rate was 46.2%. For ALS, a total of 364 miRNAs were identified in the motor cortex, 91 being up-regulated and 233 down-regulated. Target genes were predicted using miRNA bioinformatics software, and the data applied to ontology analysis. This indicated that one of the miRNAs up-regulated in ALS (miR-338-3p) had already been identified in leukocytes, serum, cerebrospinal fluid and frozen spinal cord from ALS patients.

Conclusion: Although analysis was possible for just under half of the specimens examined, we were able to show that informative miRNA data can be derived from archived FFPE samples from postmortem cases of neurodegenerative disorders.

Keywords: AMBRA1, Amyotrophic lateral sclerosis, Autophagy, Bioinformatics, Formalin-fixed paraffin-embedded specimen, MicroRNA

Introduction

MicroRNAs (miRNAs) are small, single-stranded, non-coding RNAs that regulate gene expression at the transcriptional and translational levels in both plants and animals [1]. A single miRNA may bind to as many as 200 target genes [2]. miRNAs are of great interest because they can regulate approximately 30% of human genes [3] and have a huge impact on a wide range of basic biological processes including developmental timing, cell death, cell proliferation, hematopoiesis and patterning of the nervous system [4]. The implications of miRNA network dysregulation have already been well demonstrated in the field of cancer research, suggesting that miRNAs may be good biomarkers for cancer diagnosis and prognosis [5]. The role of miRNAs has also been studied in neurodegenerative conditions such as Alzheimers disease [6-22], Parkinsons disease [19,23-27], Huntingtons disease [28-30], multiple system atrophy [31] and amyotrophic lateral sclerosis (ALS) [19,32-36], postmortem frozen brain tissue having been employed in most cases [6-22,26,28,30,31]. Several investigators have also analyzed miRNAs from cerebrospinal fluid (CSF) [6,34,37], peripheral blood [33,34,37-39] and skeletal muscle [32,35].

Although the yield, quality and integrity of RNA can be reduced through cross-linking with proteins, enzyme degradation as well as chemical degradation during the fixation process [40-44], the expression of miRNAs in formalin-fixed paraffin-embedded (FFPE) samples is known to be well correlated with that in fresh frozen samples [45]. Moreover, the expression of miRNAs is preserved after routine fixation in formalin (up to 5 days)

* Correspondence: koichi@cc.hirosaki-u.ac.jp
[1]Department of Neuropathology, Institute of Brain Science, Hirosaki University Graduate School of Medicine, 5 Zaifu-cho, Hirosaki 036-8562, Japan
Full list of author information is available at the end of the article

and long-term storage in paraffin (up to 10 years) [45]. Therefore, FFPE samples have recently been used for studies of miRNA in cancer [46-51]. However, the stability and expression of miRNAs in FFPE specimens obtained postmortem and fixed for longer time periods (weeks or months) have not been investigated.

In the present study, we isolated RNAs from archived FFPE brain specimens of postmortem cases of ALS and neurologically normal controls. Although miRNA analysis was possible for only a minority of FFPE blocks, we were able to show that informative data can be derived from selected FFPE postmortem specimens of human brain.

Materials and methods

Subjects

To investigate the effect of postmortem interval, formalin fixation and storage period on the stability of RNA, we selected 10 samples (Table 1) that had been obtained at autopsy from 1 to 10 hours after death. The brains from which the specimens had been obtained had been immersed in 10% or 20% formalin or 10% phosphate-buffered formalin for 3 16 weeks. After fixation, the cerebrum had been cut into slices 10 mm thick in the coronal plane. Samples had then been removed from each slice and subjected to tissue processing (dehydration, clearing and impregnation) on an automated instrument (Tissue-Tek VIP 5 Jr., Sakura Finetek Japan, Tokyo, Japan) that employed seven steps of 100% ethanol, three steps of xylene, and four steps of paraffin, with 8 hours at each step. The instrument was operated under vacuum and heated to 37C for the ethanol and xylene steps and 60C for the paraffin steps. After tissue processing, each specimen had been embedded in paraffin, and the paraffin blocks had been stored for 10 86 months at room temperature protected from air and sunlight.

On the basis of the criteria reported by Osawa et al. [50], four criteria were adopted for establishing the suitability of the samples for RNA analysis: (i) a postmortem interval of less than 6 hours, (ii) a formalin fixation time of less than 4 weeks, (iii) a total RNA yield per sample of more than 500 ng, and (iv) sufficient quality of the RNA electrophoresis pattern.

We further evaluated an additional 16 samples (8 cases of ALS and 8 cases of normal controls) for which the postmortem interval had been less than 6 hours and the formalin fixation time had been less than 4 weeks. Thus, we evaluated a total of 26 samples. On this basis, 10 FFPE samples were selected for miRNA analysis, comprising 6 cases of sporadic ALS and 4 neurologically normal controls (Table 2). The FFPE specimens employed were from the motor cortex of patients with ALS and normal subjects. All the diagnoses had been confirmed by neuropathological examination using immunohistochemistry for TDP-43 and ubiquitin. This study was approved by the Institutional Ethics Committee of Hirosaki University Graduate School of Medicine, Japan.

RNA extraction

Two 5-μm-thick sections were cut from each block and placed in sterile 1.5-mL centrifuge tubes ready for extraction. Tubes containing cut FFPE sections for RNA purification were stored at −80C until use. Total RNA including small RNAs was extracted using an Arcturus Paradise PLUS FFPE RNA Isolation Kit (Life Technologies Corporation, Carlsbad, CA, USA) with the following modifications. Paraffin was removed by xylene treatment and the tissues were washed with ethanol twice to remove the xylene. The tissues were then treated with proteinase K at 37C overnight, as proteinase K enables extraction of almost the same amount of RNA from FFPE specimens as from fresh frozen samples [52]. After centrifugation, the supernatant was processed with a

Table 1 Summary of fixed paraffin-embedded samples used for RNA isolation

Sample no.	Pathological diagnosis	Postmortem interval (hours)	Fixation time (weeks)	Fixative	Storage period (months)	Sample size (mm)	RNA yield (ng)
1	ALS	1	4	20% F	24	30?40	3198
2	ALS	2	4	10% BF	49	30?40	4178
3	ALS	9	8	20% F	56	30?50	911
4	ALS	9	12	20% F	10	30?50	601
5	ALS	9	16	20% F	86	25?35	515
6	ALS	4	9	10% BF	24	20?25	594
7	ALS	4	10	10% BF	12	20?20	251
8	Control	4	4	10% F	38	30?40	2769
9	Control	10	3	10% F	86	25?40	1414
10	Control	10	4	10% F	64	30?45	765

ALS, amyotrophic lateral sclerosis, F, formalin, BF, buffered formalin.

Table 2 Characteristics of postmortem cases in microRNA study

Case no.	Pathological diagnosis	Age/gender	Disease duration (months)	Postmortem interval (hours)	Fixation time (weeks)	Storage period (months)
1	ALS	68/M	12	1	4	24
2	ALS	60/M	108	2	4	49
3	ALS	59/M	36	9	8	56
4	ALS	75/M	11	4	4	36
5	ALS	73/M	9	1.5	4	60
6	ALS	72/M	120	2	4	60
7	Control	67/F		4	4	38
8	Control	71/F		10	3	86
9	Control	84/M		10	4	64
10	Control	60/F		2	4	12

silica-based spin column (Toray Industries Inc., Tokyo, Japan) in order to obtain purified total RNA. The degrees of RNA cross-linking and RNA degradation were analyzed by agarose gel electrophoresis using an Agilent 2100 Bioanalyzer (Agilent Technologies, Santa Clara, CA, USA). RNA yield was determined from the A_{260}/A_{280} absorbance ratio using a NanoDrop ND-1000 spectrophotometer (Thermo Fisher Scientific, Waltham, MA, USA).

To assess the feasibility of analyzing RNA extracted from FFPE samples, we applied the selection criteria for RNA quality reported by Osawa et al. [50], as described above. The RNA electrophoresis pattern was found to be crucial for estimation of RNA quality. When the majority of RNAs were >4000 nucleotides (nt) in size due to cross-linking or when almost all of the RNAs were fragmented (e.g., <1000 nt), the RNA quality was considered unsuitable for miRNA analysis.

miRNA expression profiling

Extracted samples of total RNA that satisfied our criteria were labeled with Hy5 using a miRCURY LNA Array miR labeling kit (Exiqon, Vedbaek, Denmark). The labeled RNAs were then hybridized onto a 3D-Gene human miRNA oligo chip (Toray Industries Inc.). The annotation and oligonucleotide sequences of the probes conformed to the miRBase miRNA database Release 17v1.0.0 (http://www.mirbase.org/). After stringent washing, the fluorescent signals were scanned with a 3D-Gene Scanner (Toray Industries Inc.) and analyzed using 3D-Gene Extraction software (Toray Industries Inc.).

The raw data for each spot were normalized by subtraction of the mean intensity of the background signal determined from the signal intensities of all blank spots with 95% confidence intervals. Measurements for spots with signal intensities greater than 2 standard deviations (SD) of the background signal intensity were considered to be valid. The relative level of expression for a given miRNA was calculated by comparing the signal intensities of the valid spots throughout the microarray experiments. The normalized data were globally normalized per array, adjusting the median of the signal intensity to 25.

Any signal intensity level over 50 was considered to be significant. The signal was considered to be up-regulated when $\log_2 X$ was increased by 0.1 or more ($\geq \log_2 X = +0.1$) compared with the control signal level, and down-regulated when $\log_2 X$ was decreased by −0.1 or less ($\leq \log_2 X = -0.1$) compared with the control signal level.

miRNA targets and pathway analysis

Bioinformatics prediction of target genes and miRNA binding sites was performed using miRmap web-based open source software (http://mirmap.ezlab.org/) [53]. Canonical function and ontology analyses for candidate miRNA targets were performed using MetaCore Functional Analysis (ver.6.19, Thomson Reuter/GeneGo, http://lsresearch.thomsonreuters.com/) which is an integrated knowledge base and pathway analysis tool based on a proprietary manually curated database of human protein protein, protein DNA and protein compound interactions, and metabolic and signaling pathways, all supported by proprietary ontologies. Gene ontology enrichment analysis was also performed with Gene Ontology Consortium (GOC) web tool (http://geneontology.org/) to confirm standard GO term on the coincidences.

Immunohistochemistry

Since *SOGA1* (suppressor of glucose by autophagy) [54] was identified as one of the candidate target genes of both up-regulated and down-regulated miRNAs, we evaluated the protein expression levels of autophagy-related genes such as AMBRA1 [55], Beclin 1 [56], ULK1 [57] and ULK2 [57] using immunohistochemistry. Serial 4-μm-thick FFPE sections from the motor cortex and spinal cord (7th cervical, 8th thoracic and 4th lumbar segments) of ALS patients (n = 13) were employed. We also examined neurologically normal individuals (normal control) (n = 6) and patients with various neurological diseases affecting the spinal anterior horn (diseased control) (n = 6). Three sections 40 μm apart were subjected to immunohistochemistry using the avidin-biotin-peroxidase complex method with a Vectastain ABC kit (Vector, Burlingame, CA, USA). The sections were subjected to heat retrieval using an autoclave for 10 min at 121C in 10 mM citrate buffer (pH 6.0), and then immunostained with rabbit polyclonal antibodies against AMBRA1 (NOVUS USA, Littleton, CO, USA; 1:1000), Beclin 1 (NOVUS USA; 1:200), ULK1 (Thermo Scientific, Rockford, IL, USA; 1:100) and ULK2 (Thermo Scientific; 1:500). Diaminobenzidine was used as the chromogen, and the sections were counterstained with hematoxylin.

Semi-quantitative analysis

Since AMBRA1 immunoreactivity was decreased in the spinal anterior horn cells in ALS, we assessed the number of AMBRA1-immunoreactive neurons in the spinal anterior horn of control subjects and patients with ALS using a semi-quantitative rating scale, as reported previously [58]: −, unstained; +, weakly stained; ++, moderately or intensely stained. In each case, the numbers of neurons were counted in Rexed s laminae VIII and IX of the lumbar spinal cord. Counting was performed at an original magnification of x200 using an eyepiece graticule and parallel sweeps of the microscope stage.

Statistical analysis

Calculations were performed using Statcel software (OMS Publishing, Tokorozawa, Japan). Repeated measures analysis of variance and Student s or Welch s *t* test were used to evaluate possible differences in staining intensity between normal controls, diseased controls and ALS. Values were expressed as mean standard error of the mean. Correlations at $p < 0.05$ were considered to be significant.

Results

Stability of RNA in postmortem samples

The RNA yield was not correlated with the period of storage of FFPE blocks. However, the RNA yield was influenced by the period of formalin fixation (Table 1), being significantly higher in samples that had been fixed for a short period (3 4 weeks; mean 2465 ng) than in those that have been fixed for a long period (8 16 weeks; mean 574 ng) ($p < 0.05$). The RNA yield did not appear to be affected by the type of fixative employed. Postmortem interval could be also relevant. Samples with higher RNA yield (samples 1, 2 and 8) were the cases in whom postmortem interval was within 4 hours. The rest with lower RNA yield (samples 3 7, 9 and 10) had a combination of longer postmortem interval (9 10 hours) and/or fixation (8 16 weeks). RNA integrity was checked by electrophoresis, and a representative RNA agarose gel image is shown in Figure 1. A band of 5000 nt corresponding to 28S ribosomal RNA was slightly shifted toward a higher molecular weight in all cases, indicating overfixation with formalin and the presence of chemical modifications of the RNA such as covalently linked residual amino acids [59]. A band of 2000 nt corresponding to 18S ribosomal RNA was seen in some cases (Figure 1), suggesting that the extracted RNA was of good quality. These bands were not only shifted, but also appeared more diffuse and less focused. The bands of 100 200 nt corresponded to degraded RNA, as reported previously [60]. On the basis of these

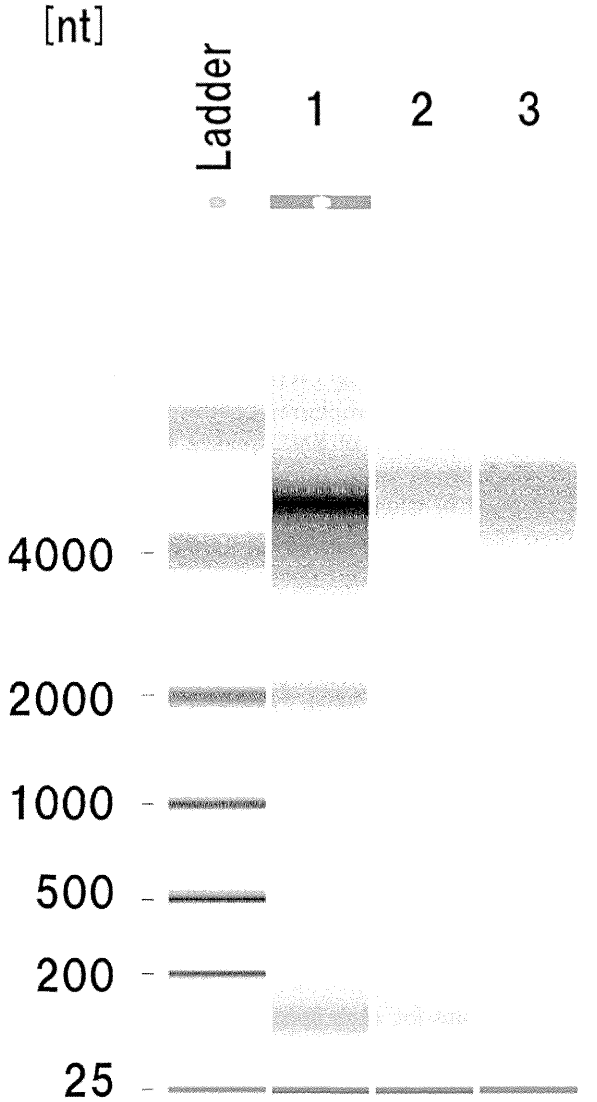

Figure 1 Effect of formalin fixation on RNA expression. Representative RNA agarose gel image showing a band of 2000 nt corresponding to 18S ribosomal RNA in lane 1. A faint band of 2000 nt is also seen in lanes 2 and 3. Lane 1, sample 2; lane 2, sample 1; lane 3, sample 8.

initial analyses, we adopted four criteria to indicate that RNA would be of sufficient quality for analysis, based on Osawa et al. [50]: (i) a postmortem interval of less than 6 hours, (ii) a formalin fixation time of less than 4 weeks, (iii) a total RNA yield per sample of more than 500 ng, and (iv) a RNA electrophoresis pattern of good quality.

We evaluated an additional 16 samples (8 cases of ALS and 8 cases of normal controls) for which the postmortem interval had been less than 6 hours and the formalin fixation time had been less than 4 weeks. The RNA yield was more than 500 ng for 12 of these samples, and the RNA agarose gel image was of sufficient quality in 4. As a result, we evaluated a total of 26 samples. The RNA yield was more than 500 ng in 20 of the 26 samples, and the RNA agarose gel image was of sufficient quality in 12. Thus, the success rate for analysis of RNA from FFPE samples of the human postmortem brain was 46.2% (12 of 26).

Based on the above step, 10 cases were selected for miRNA analysis; these included cases of sporadic ALS (n = 6) and neurologically normal controls (n = 4) (Table 2). In case 3, although the fixation time had been 8 weeks, it was included in the present analysis, because the RNA yield was more than 500 ng and the RNA agarose gel image was of sufficient quality.

miRNA analysis and candidate target genes in ALS

A total of 364 miRNAs were isolated from the motor cortex of patients with ALS. Forty miRNAs showed no change ($-0.1 < \log_2 X < +0.1$), and 91 were up-regulated ($\log_2 X \geqq +0.1$) and 233 were down-regulated ($\log_2 X \leqq -0.1$) relative to the controls. Top 20 microRNAs up- or down-regulated in ALS are shown in Additional file 1: Table S1. miR-494 was found to be the most highly differentially up-regulated miRNA (+4.99-fold change), followed in order by miR-4257, miR-24-3p, miR-4299, and miR-1973 as the top 5 up-regulated miRNAs. On the other hand, miR-4740-5p (+0.19-fold change), miR-1290, miR-3619-3p, miR-1246, and miR-3180-3p were the top 5 down-regulated miRNAs.

Scatter plot of all 364 miRNAs comparing signal intensity versus $\log_2$ fold-change of ALS/control ratio is shown in Figure 2. We selected 6 up-regulated miRNAs (miR-494, miR-4257, miR-24-3p, miR-4299, miR-1973 and miR-4485) and 8 down-regulated miRNAs (miR-4740-5p, miR-1290, miR-3619-3p, miR-1246, miR-3180-3p, miR-4648, miR-4716-3p and miR-663) in ALS. The candidate target genes of the 6 up-regulated and 8 down-regulated miRNAs in ALS were identified using miRmap web-based open source software.

Top 50 candidate target genes of each of the 6 up-regulated miRNAs in ALS were selected according to the miRmap score. Of the 300 target candidates identified for each of the 6 miRNAs, there was an overlap of 13 genes (Additional file 2: Table S2). These 13 genes have been reported to be involved in muscular cell proliferation (FOXK1 [61], MEF2D [62]), synaptic transmission (ITSN1 [63], RAB3B [64], SLC6A5 [65]), mitochondrial regulation (IBA57 [66], PPARGC1B [67]) and autophagy (MEF2D [68], SOGA1 [54]). These genes may be down-regulated by the 6 up-regulated miRNAs in affected brain regions of ALS. In addition, miR-24-3p showed the most matching frequency (7 overlapped in 50 targets) in up-regulated miRNAs.

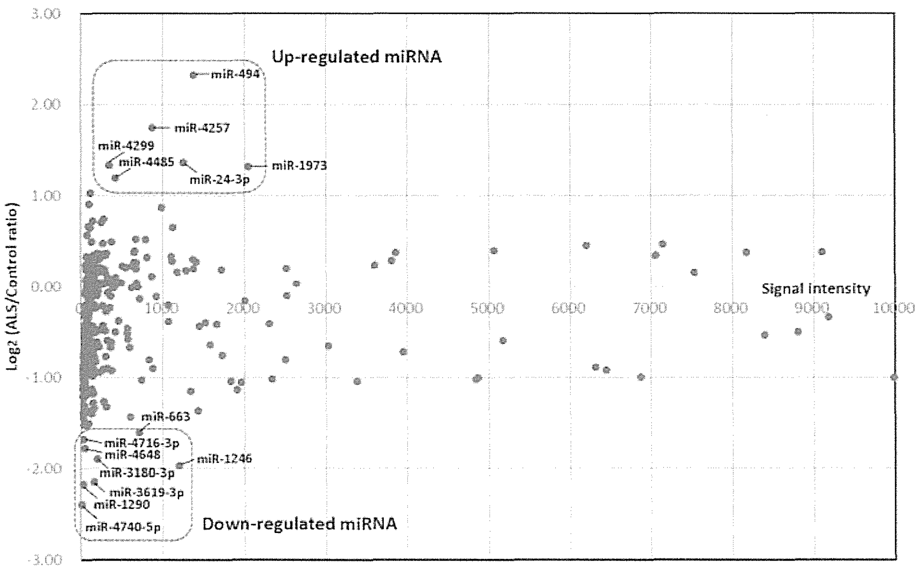

Figure 2 Scatter plot of all 364 miRNAs comparing signal intensity (X-axis) versus $\log_2$ fold-change of amyotrophic lateral sclerosis (ALS)/control ratio (Y-axis). Based on the size of variation, 6 up-regulated and 8 down-regulated miRNAs were selected in ALS.

Top 50 candidate target genes of each of the 8 down-regulated miRNAs in ALS were also selected. Of the 400 target candidates identified for each of the 8 miRNAs, there was an overlap of 34 genes (Additional file 3: Table S3). These 34 genes have been reported to play a role in neurogenesis (ONECUT2 [69], KDM5A [70], NAT8L [71], NFIX [72]), mitochondrial regulation (IBA57 [66]) and autophagy (PRLA [73], SNCB [74], SOGA1 [54]). In addition, miR-3180-3p showed the most matching frequency (14 overlapped in 50 targets) in down-regulated miRNAs.

It is important to note that 3 genes (*IBA57*, *RAB3B* and *SOGA1*) were identified as candidate target genes of both up-regulated and down-regulated miRNAs (Additional file 2: Table S2, Additional file 3: Table S3). *IBA57* is known to be involved in the biosynthesis of mitochondrial [4Fe-4S] proteins [66]. Mutation of *IBA57* causes severe myopathy and encephalopathy [66]. Rab3B is a synaptic vesicle protein that interacts with the Rab3-interacting molecule isoforms as effector proteins in a GTP-dependent manner [64]. The search for an inhibitor of autophagy in the adiponectin signaling pathway led to the discovery of the Suppressor of Glucose from Autophagy (SOGA) [54]. These findings suggest that mitochondrial regulation, synaptic transmission and autophagy may be affected in ALS. Considering that the expression level of up-regulated miRNAs is higher than that of down-regulated miRNAs (Figure 2), these 3 genes may be down-regulated in the motor cortex of ALS.

Gene ontology analysis of predicted target genes for disease-specific miRNAs

A total of 300 candidates for 6 up-regulated miRNAs and 400 candidates for 8 down-regulated miRNAs were nominated as targets for gene ontology enrichment analysis (biological process). Additional file 4: Table S4 (A, B) shows top 10 GO terms with MetaCore analysis and Additional file 4: Table S4 (C, D) shows top 10 GO terms with GOC analysis for standard GO terms. Two GO analyses suggested essentially similar biological process in up-regulated and down-regulated miRNA target genes.

The biological processes in ALS altered by these target genes were shown to be related to protein transport, synaptic vesicle-mediated transport, and localization for up-regulated miRNAs and nervous system development for down-regulated miRNAs, as shown in Additional file 4: Table S4.

Decrease of AMBRA1 immunoreactivity in ALS

Since *SOGA1* was identified as one of the overlapped target genes predicted by 6 up-regulated and 8 down-regulated miRNAs, we hypothesized that alteration of autophagy is involved in the disease process of ALS. This may be supported by the findings that abnormal autophagy is involved in various neurodegenerative disorders, including ALS [75-79]. Therefore, we evaluated the protein expression levels of autophagy-related genes such as AMBRA1 [55], Beclin 1 [56], ULK1 [57] and ULK2 [57] by immunohistochemical examination of FFPE tissue.

In specimens from normal control subjects, anti-AMBRA1 antibody strongly immunolabeled the cytoplasm of upper and lower motor neurons in a diffuse granular pattern (Figure 3A-C), consistent with a previous study [80]. In ALS, AMBRA1 immunoreactivity was decreased in the majority of spinal anterior horn cells (Figure 3D-F), but not in the motor cortex (data not shown), in comparison with controls.

Semi-quantitative analysis of normal controls showed that 30.2% of anterior horn cells were moderately or intensely immunolabeled, 48.5% were weakly immunolabeled, and 21.3% were unstained (Figure 4). Similarly, in diseased controls, 20% of anterior horn cells were moderately or intensely immunolabeled and 33.7% were weakly immunolabeled (Figure 4). The differences in staining intensity between normal and diseased controls were not statistically significant. In ALS, a small proportion of anterior horn cells (5.2%) showed moderate or intense immunoreactivity, whereas the majority (83.5%) were unstained (Figure 4). The differences in staining intensity between normal control and ALS cases and between diseased control and ALS cases were significant.

Immunoreactivity for Beclin 1, ULK1 and ULK2 was observed in the neuronal cytoplasm in normal controls. No significant difference was found in the staining intensity of these proteins between ALS and normal controls (data not shown).

Discussion

It has been reported that the formalin fixation and paraffin embedding process results in a marked reduction of detectable mRNA [81]. This process causes enzymatic degradation and chemical modification of RNA giving rise to cross-links with proteins and making RNA extraction difficult [52]. Therefore, a digestion step with proteinase K is required to eliminate cross-links and facilitate RNA extraction from FFPE samples [52]. The longer an RNA molecule is, the more likely cross-links will remain after proteinase K digestion, hence small RNA molecules will be easier to extract from FFPE samples and fragments larger than 200 nt will be harder to recover from FFPE samples. In addition, electrophoretic profiles of total RNA from frozen samples show three characteristic peaks: 40 80 nt, 90 nt and 150 nt, probably corresponding to tRNAs, rRNAs and snoRNAs, respectively. On the other hand, FFPE sample shows an accumulation of RNA fragments smaller than 200 nt [82]. These findings suggest that the amount of total RNA that can be extracted from a FFPE tissue sample is

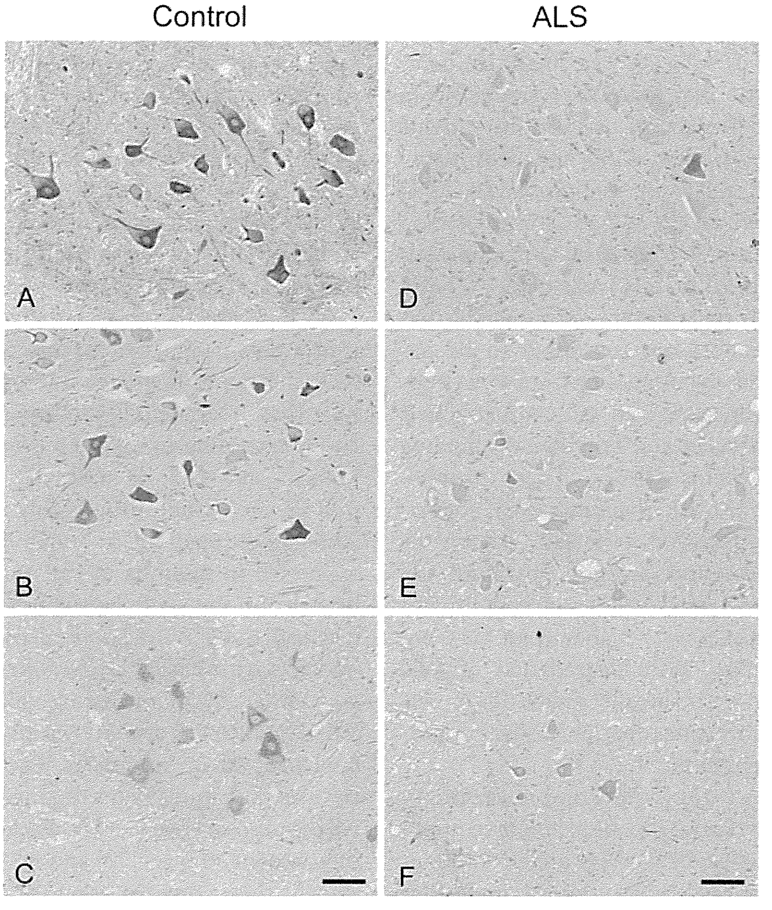

Figure 3 AMBRA1 immunoreactivity in the anterior horn of the lumbar cord in 3 normal controls (A-C) and 3 cases of ALS (D-F). AMBRA1 immunoreactivity is decreased in ALS relative to the controls. Bars = 100 μm.

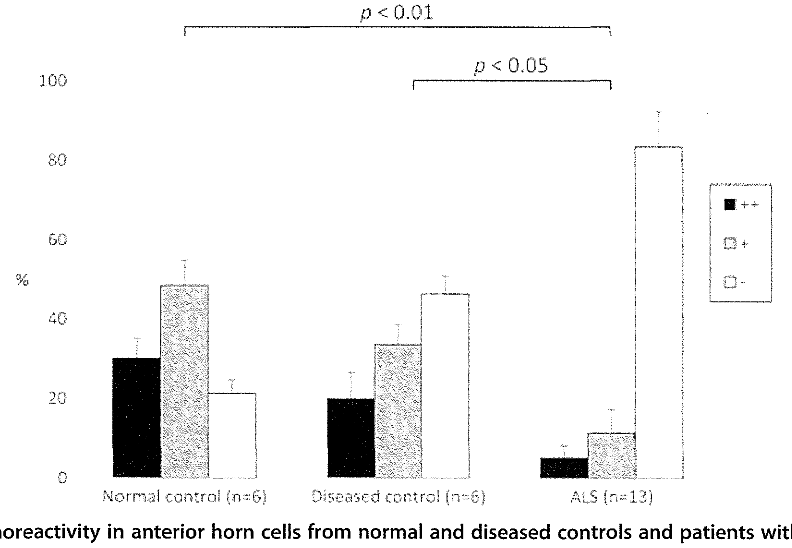

Figure 4 AMBRA1 immunoreactivity in anterior horn cells from normal and diseased controls and patients with ALS. The proportions of neurons showing intense/moderate (++, black column), weak (+, gray column), or no immunostaining for AMBRA1 (–, white column) relative to the total number of neurons in the anterior horn are indicated.

only a fraction of what can be extracted from its corresponding frozen tissue [81].

Although the number of subjects was small, we demonstrated for the first time that miRNAs extracted from FFPE samples of postmortem brain tissue from patients with neurodegenerative disorder (ALS) and neurologically normal controls were relatively well preserved; 12 of 26 samples (46.2%), for which the longest storage period was more than 7 years, provided RNA of sufficient quality. Thus, miRNAs appear to be relatively stable in FFPE samples, even those from postmortem specimens. It has been suggested that miRNAs are too small to be degraded [83]. However, this hypothesis has not been supported by any reported data. It is now known that active, mature miRNAs are processed and function via binding to Argonaute family proteins [84,85]. These protein-miRNA complexes may protect the functional population of miRNA from degradation, especially during the process of formalin fixation and storage in paraffin [49]. Peir-Chova et al. [82] have shown that the quantity of miRNAs from FFPE samples was higher than that obtained from frozen samples, since degradation of total RNA can produce fragments in the small RNA size range that could cause an overestimation in the proportion of its small sized fragments.

ALS is characterized by loss of upper and lower motor neurons. TDP-43 is now known to be a major component of ubiquitinated inclusions in ALS and frontotemporal lobar degeneration with ubiquitinated inclusions (FTLD-U, since renamed FTLD-TDP) [86,87]. Thus, these neurodegenerative disorders comprise a new disease concept: TDP-43 proteinopathy . Up- or down-regulated miRNAs in ALS in the present study and previously reported results are shown in Additional file 5: Table S5. Williams et al. [36] compared miRNA expression in skeletal muscle of normal and ALS model mice (G93A-SOD1 transgenic mice) and demonstrated that miR-206, a skeletal muscle-specific miRNA in humans and mice, delays disease progression in SOD1 transgenic mice. miR-206 is up-regulated in the skeletal muscle of ALS patients [32]. Shioya et al. [19] studied the miRNA expression profile in frozen samples of frontal cortex from three ALS patients using microarray analysis and found that miR-29a, miR-29b and miR-338-3p were up-regulated. Up-regulation of miR-29b has also been reported in skeletal muscle of ALS patients [35]. De Felice et al. [33] evaluated miRNA expression in leukocytes obtained from ALS patients and healthy controls and demonstrated that miR-338-3p was also up-regulated in ALS. Seven miRNAs (miR-451, miR-1275, miR-328, miR-638, miR-149, miR-665 and miR-583) were also down-regulated in ALS. Importantly, in our present study, three miRNAs (miR-29a, miR-29b and miR-338-3p) were also up-regulated and four miRNAs (miR-328, miR-451, miR-638 and miR-665) were down-regulated in FFPE samples of the motor cortex in ALS. Recently, De Felice et al. [34] further demonstrated that miR-338-3p was over-expressed in leukocytes, serum, CSF and frozen samples of spinal cord in patients with ALS, and that miR-338-3p expression in leukocytes was correlated with disease duration, suggesting that miR-338-3p may be a relevant clinical biomarker of ALS. It is likely that some miRNAs are systemically dysregulated in ALS and that miRNAs remain stable even in FFPE postmortem samples that have been stored for a long period.

We further demonstrated that AMBRA1 was significantly down-regulated in the lower motor neurons in ALS. This is in line with the results of our miRNA analysis that AMBRA1 is most possibly regulated by miR-24-3p according to miRmap prediction (the rank 1 in canonical miRNAs of miRmap score = 97.37) and that miR-24-3p is one of the highly up-regulated miRNAs in ALS (Additional file 1: Table S1). AMBRA1 is widely expressed in neurons in the normal mouse brain and is localized to the endoplasmic reticulum, perinuclear cisternae and outer mitochondrial membrane [80]. AMBRA1 interacts with Beclin 1, promoting its binding to lipid kinase Vps34, thus mediating autophagosome nucleation [55]. AMBRA1 is also known to be a Parkin-binding protein involved in mitophagy [88]. Abnormal autophagy is involved in various neurodegenerative disorders, including Alzheimer s disease [75,76], Parkinson s disease [78], multiple system atrophy [79] and ALS [77]. A recent study has shown that administration of rapamycin, an MTOR-dependent autophagy activator, ameliorates neuronal degeneration in FTLD-TDP model mice [89]. By contrast, rapamycin also aggravates neuronal death in a mouse model of ALS [90]. Thus, induction or repression of autophagy should be taken into account when considering novel therapeutic approaches for TDP-43 proteinopathy.

Conclusion

In conclusion, we have utilized FFPE brain samples from postmortem cases of ALS and neurologically normal controls and found that miRNAs extracted from these samples were relatively well preserved. Although further studies with a larger sample size are necessary, it is likely that archived FFPE postmortem samples can be a valuable source for miRNA profiling in neurodegenerative disorders.

Additional files

Additional file 1: Table S1. Top 20 microRNAs up- or down-regulated in the motor cortex in ALS.

Additional file 2: Table S2. Predicted target genes for ALS-specific up-regulated miRNAs identified by miRmap web-based open source software.